



**BEDFORMS IN WAVE-FORCED NEARSHORE ENVIRONMENTS:
OBSERVATIONS WITH A PROTOTYPE HUMAN-POWERED SURFACE
VEHICLE**

Kara A. Vogler

SUBMITTED IN PARTIAL FULFILLMENT OF THE REQUIREMENTS
FOR THE DEGREE OF BACHELOR OF SCIENCES, HONOURS
DEPARTMENT OF EARTH SCIENCES
DALHOUSIE UNIVERSITY, HALIFAX, NOVA SCOTIA

April 2017

Abstract

Bedforms in nearshore environments are undulatory sedimentary structures formed by wave-forced fluid-sediment interactions at the seabed. Signature characteristics imprinted on the sediment fabric may be used to infer environmental conditions in the past by comparison to bedforms in the geologic record. Lunate megaripples and cross-ripples are bedforms with complex geometries that have been observed in nearshore environments, however they are not well studied in the literature and the conditions required for their formation are unclear. Previous surveying methods have recorded observations using instruments installed in the seafloor, which can disturb the sediment and obstruct fluid flow. The purpose of this study is to refine methodology for observing lunate megaripples and cross-ripples non-invasively. The study site, Crystal Crescent Beach, in Sambro, Nova Scotia, was selected for its sandy bottom and clear water. A low cost, human-powered surface vehicle was constructed using a surfboard as the platform for mounting (1) a video imaging device to record bedform morphologies at varying depths, and (2) a sonar device connected to GPS to detect and document ocean floor topography. Surveys were conducted prior to a storm event, during the event, then after the event to observe bedform transformation. Sand samples were obtained for analyzing grain size characteristics of the bedforms. Weather, wind, and wave conditions were recorded before, during, and following fieldwork to document potential physical conditions associated with bed geometries. Still frames from videos of pre-storm seabed conditions compared to videos of post-storm conditions showed recognizably different bedforms. In videos acquired during the storm, suspended sediment in the water column made it difficult to observe the seafloor. Analysis of weather data confirmed that large wave heights were associated with high wind speed, and grain size analysis showed that more complex, three-dimensional bedforms occurred where there was variability in grain size. Figures created using sonar data illustrated an overall change in beach geometry throughout the storm event. Overall, observations were relatively high quality, allowing for identification distinct ripple geometries and change in overall bed state associated with growth and decay of storm wave conditions. This study demonstrated potential for examining bedforms using low-cost, human-powered, instrumented surface vehicles. Therefore, despite being an initial attempt, this study can be used as a basis for further studies of bedform development in nearshore environments.

Keywords: Bedform, lunate megaripple, cross ripple, high energy, nearshore

Table of Contents

Abstract	i
Table of Contents	ii
Table of Figures	iv
List of Tables	vii
Acknowledgements	viii
Chapter 1: Introduction	1
1.1 Introduction	1
1.2 Previous Work and Background Information	2
1.3 Thesis Objective: Purpose of the Study	5
Chapter 2: Geological Setting and Study Site	7
Chapter 3: Methodology	9
3.1 Preparation for Fieldwork	9
3.1.1 Constructing the Surface Vehicle	9
3.1.2 Weather and Wave Condition Data	11
3.2 Field Technologies	12
3.2.1 Deeper Fishfinder 3.0 Sonar	12
3.2.2 GoPro HERO3 Video Camera	13
3.3 Data Collection and Procedure in the Field	13
3.3.1 Sand Sampling	13
3.3.2 Depth Data and GoPro Video Collection	14
3.4 Data Analysis Methods	16

3.4.1 Weather Data Analysis	16
3.4.2 Sand Sample Preparation and Sieving	17
3.4.3 GoPro HERO3 Video Analysis	18
3.4.4 Deeper Fishfinder 3.0 Data Analysis	20
Chapter 4: Results	21
4.1 Weather and Sea Conditions	21
4.2 Grain Size	23
4.3 Deeper 3.0 Fishfinder Data	25
4.4 GoPro Videos: Observations and Images	31
Chapter 5: Discussion	37
5.1 Bedforms Observed and Interpretation	37
5.2 Deeper Fishfinder 3.0 Sonar	41
5.3 Challenges	42
Chapter 6: Summary and Conclusions	44
Referenced Literature	46
Appendix A	48
Appendix B	58
Appendix C	62

Table of Figures

Chapter 1: Introduction

Figure 1.1	Ripple marks indicative of wave dominated deltaic environments	1
Figure 1.2	Progression of bedform geometries	2
Figure 1.3	Sketch of cross-ripples sketch of lunate megaripples	3
Figure 1.4	Fan beam sonar apparatus	4

Chapter 2: Geological Setting and Study Site

Figure 2.1	Crystal Crescent Beach	7
Figure 2.2	Study Site	8

Chapter 3: Methodology

Figure 3.1	State of the surfboard as received	9
Figure 3.2	Completed surfboard-surface-vehicle	10
Figure 3.3	Images from Windytv weather projections	12
Figure 3.4	Deeper Fishfinder sending out sound waves	13
Figure 3.5	GoPro Hero3 in submersible case	14
Figure 3.6	Surfboard-surface-vehicle set-up with field materials	15
Figure 3.7	Photos showing various field procedures	16
Figure 3.8	Sand samples obtained from varying water depths including	17
Figure 3.9	Series of enhancements made to GoPro still frames	18
Figure 3.10	Video images of a checkerboard used for calibrating the GoPro	19
Figure 3.11	Calculating scale for GoPro stills	20

Chapter 4: Results

Figure 4.1	Wave height versus horizontal wind speed	22
Figure 4.2	Wind direction versus wind speed	22
Figure 4.3	Atmospheric pressure versus wind speed	23
Figure 4.4	Grain size distribution histograms and photos	24
Figure 4.5	Traverse paths during each survey	25
Figure 4.6	Swim path superimposed on Google Earth image	26
Figure 4.7	Bathymetry: November 15, 2017	27
Figure 4.8	Bathymetry: November 17, 2017	28
Figure 4.9	Bathymetry: November 26, 2017	29
Figure 4.10	Flattened representation of the depth	30
Figure 4.11	1m depth: Somewhat lunate ripples	32
Figure 4.12	1m depth: Low amplitude/planar ripples	32
Figure 4.13	1.5m depth: Three-dimensional ripples	32
Figure 4.14	1m depth: Small plants in the seabed surrounded by complex crossing of bedforms and irregular cross ripples	33
Figure 4.15	1m depth: Highly turbid water near the swash zone	33
Figure 4.16	1.5m depth: 'Domes and depressions', lunate ripples	33
Figure 4.17	2m depth: Somewhat lunate, 3D ripples Isolated cross ripples	34
Figure 4.18	2.5 m depth: Transition towards longer, more continuous bedforms	34
Figure 4.19	2m depth: Regular cross ripple structures creating diamond shapes	35
Figure 4.20	2m depth: Continuous, sinuous, long-crested ripples	35
Figure 4.21	3.5m depth: Long-crested, straight ripples with bifurcations	36

Figure 4.22	3m depth: Very turbid water column	36
Figure 4.23	3m depth. Straight, continuous ripples with bifurcations, Isolated short-crested ripples in the troughs of other ripples	37

Chapter 5: Discussion

Figure 5.1	Sketch of cross-rippled bed with two long-crested components oriented at $\pm 30^\circ$	39
Figure 5.2	Schematic diagram of obstacles and cross ripple formation	40
Figure 5.3	Schematic diagram of waves interacting with the seabed	41
Figure 5.4	Sketch showing positioning of Deeper Fishfinder sonar relative to the seafloor	42

List of Tables

Table 1	Websites used to collect weather data	11
Table 2	Average of hourly wave heights from NOAA buoy C44137.	21

Acknowledgements

We all harbour great curiosity for the wonders of the incredible planet around us. This honours thesis speaks to exploring curiosity, and is dedicated to all those who have made my unusual endeavours a reality. I am deeply grateful and would like to acknowledge each person who bore patiently with my persistence.

I cannot find enough gratifying words to thank Dr. Alex E. Hay, who, with great enthusiasm, presented me with the opportunity to apply my skills, interest in science, and love for the ocean to a realistic, explorative opportunity. I thank, with sincere appreciation, Mr. Richard Cheel for his inexhaustible patience, direction and mentoring, and sharing of his fieldwork and technological expertise.

I wholeheartedly thank Ms. Catie Heym, who, as a kind friend, often came to my rescue, spending long hours sorting out my computer woes. I am grateful for the encouragement of advisor Michael Young and Professor Djordje Grujic for their reassurance and enthusiasm. Mr. Gavin McNamara and Mr. Oliver Blume, I express gratitude for their help and endurance, accompanying me to the field in the brisk, stormy autumn weather.

Finally, I thank my family for their endless support, love, and willingness listen and offer help in any way they can.

Chapter 1: Introduction

1.1 Introduction

Bedforms are wave-generated sedimentary structures formed in high-energy environments by fluid-sediment interactions at the seabed. Signature bedform geometries are shaped by specific hydrodynamic conditions. The importance of studying bedforms in modern environments pertains to their presence in the stratigraphic record (Figure 1.1). These sedimentary structures reflect flow parameters, such as velocity and direction of oscillatory currents, horizontal component of orbital motion, and velocity asymmetry (Clifton & Dingler 1984). Since the present is the key to the past (Hutton & Craig 1987), understanding the influence of wave forcing on the seabed is vital for interpreting depositional environments in geologic history (Clifton et al. 1971).

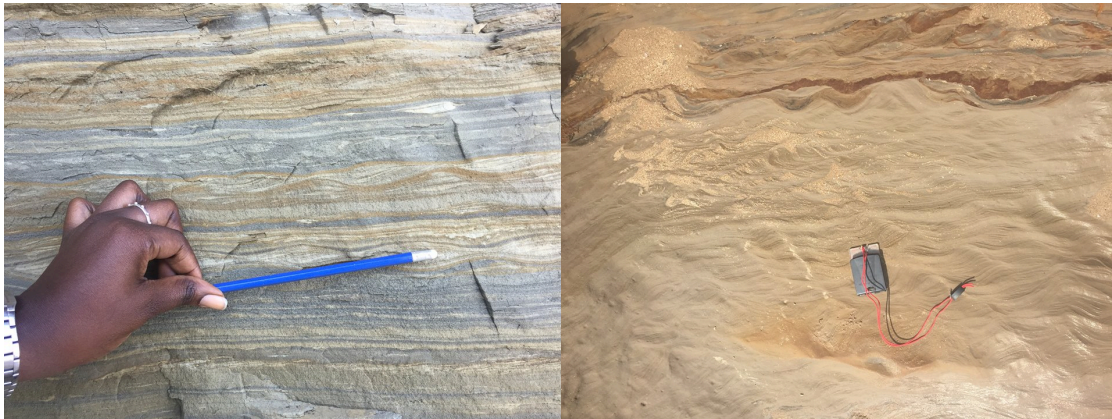


Figure 1.1 Ripple marks indicative of wave dominated deltaic environments preserved in Pliocene-aged sediments. (Left) Photo from the cliffs of Cedros Bay, Bonasse, Trinidad. 15cm pencil for scale. (Right) Photo from the cliffs of Mayaro Beach, Trinidad. Suunto Compass (10cm in length) for scale.

Nearshore environments are characterized by a distinct, interrelated depositional regime defined by different zones of wave action. Clifton et al. (1971) first described this phenomenon as having a shoreward progression due to shoaling waves. Bedform geometries evolve as waves increase in energy while approaching the shore, steepen, and eventually break. Figure 1.2, from Cheel (2007), shows long-crested ripples furthest from shore, then irregular ripples where long crests break apart, then cross

ripples, lunate megaripples, and finally flat bed, occurring where waves break at the shoreline. This progression of bed state and ripple formation has been observed repeatedly in studies of nearshore environments.

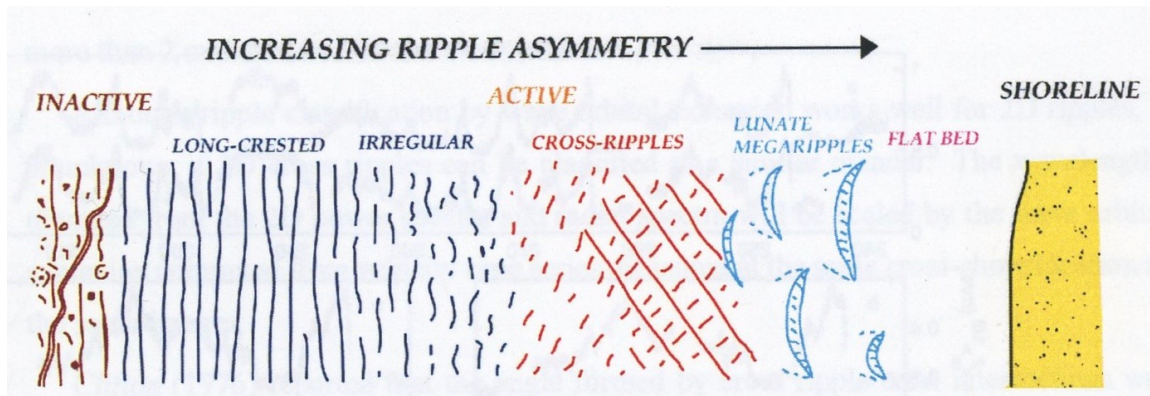


Figure 1.2 Progression of bedform geometries as waves approach the shoreline from offshore (Cheel 2007) .

Lunate megaripples and cross-ripples are bedforms with complex structures that have been observed in the nearshore depositional regime. Cross ripples occur outside of the surf zone during phases of wave growth and decay associated with storm events (Cheel & Hay 2008). They are characterized by a ladder-like appearance (Cheel & Hay 2008) consisting of short-crested ripples within the troughs of long-crested ripples (Figure 1.3(1)), where ripple crests intersect at approximately 90° (Cheel 2007). Lunate megaripples are asymmetric, landward facing, crescentic bedforms (Figure 1.3(2)) occurring beneath the zone of wave build-up (Clifton et al. 1971). They tend to be oriented oblique to the flow direction, and open towards the shore (Clifton & Dingler 1984). Once formed, lunate megaripples persist through a wide range of forcing conditions, suggesting a longer response time and evolution out of equilibrium with wave forcing (Hay & Mudge 2005).

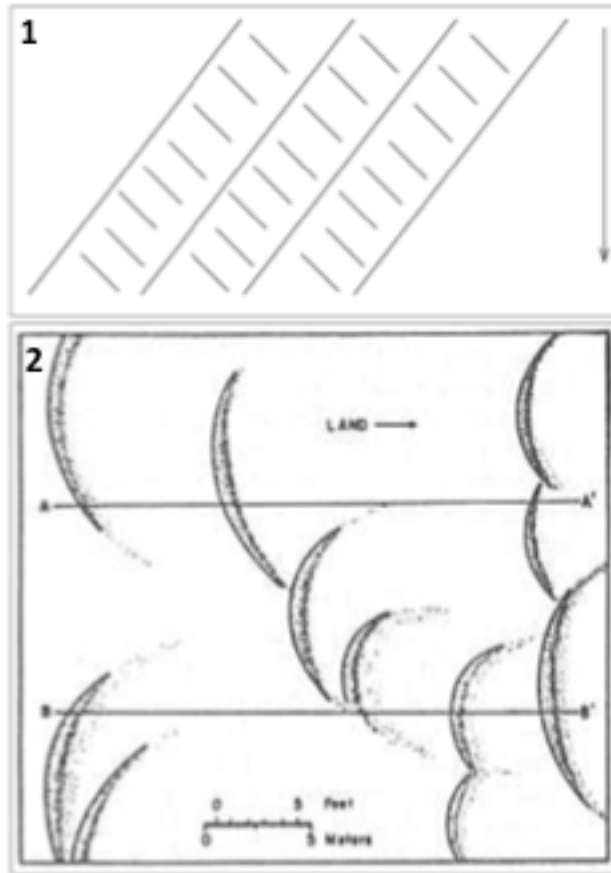


Figure 1.3 (1) Representative sketch of cross-ripples in plan view, emphasizing ladder-like appearance and arrangement. Flow direction indicated by the arrow (Cheel & Hay 2008). (2) Drawing of lunate megaripple geometries in plan view (Clifton et al. 1971).

1.2 Previous Work and Background Information

1971 study by Clifton et al. on bedform geometries in high-energy nearshore environments utilized SCUBA techniques to collect observations of bedforms. Other experimental methodology included a nylon line fixed at the shore, used to measure distance from the shoreline, and a stadia rod for depth measurements. The study was conducted in non-storm summer conditions. Researchers were able to discern a repeated shoreward progression of depositional facies, including: asymmetric ripples furthest from shore; lunate megaripple; an outer planar facies characterized by either broad gentle undulations or long-crested, short wavelength ripples; an area of irregular bedforms between the surf and swash zone; and an inner planar facies located at the

swash zone, described by a planar surface. This study focused on describing the internal structures of each facies and how they might be recognized in the geologic record.

Clifton (1976) strove to develop a model to provide a baseline for hydrodynamic interpretation of bedforms by integrating observations of structures from multiple depositional environments. He observed that the shoreward progression of facies was governed by sediment grain size, as well as changes in the properties of wave forcing as waves approached the shore. Cross ripple geometry was addressed, but the conditions for their formation were not understood. This study explored how the transition from asymmetric ripples to symmetric ripples in modern environments could be used to determine water depths in the geologic record. Clifton and Dingler (1984) considered how the results of laboratory studies might be misleading, as long-period oceanic waves are difficult to replicate. Their study incorporated mathematic wave equations from various wave theories – including Airy, Stokes, cnoidal, and solitary wave theory – to

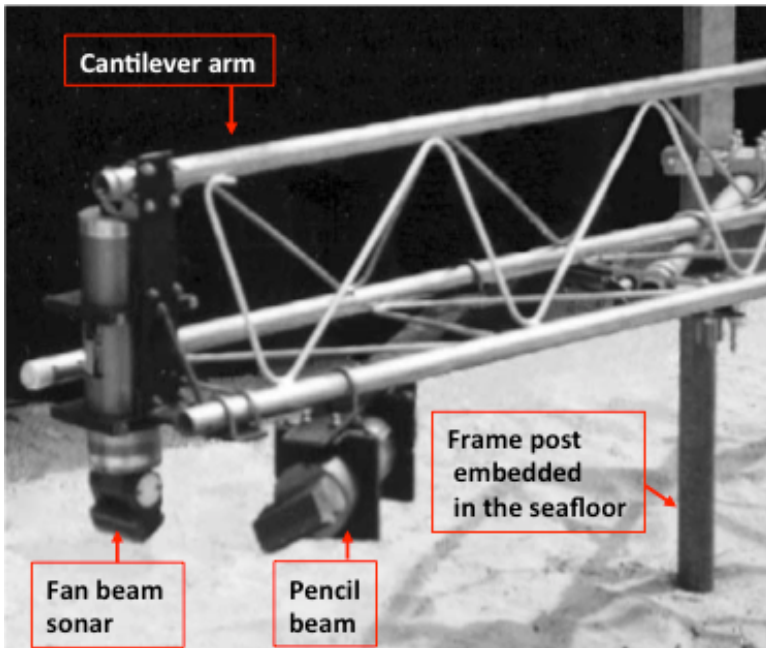


Figure 1.4 Photo of fan beam sonar apparatus from Hay and Mudge (2005). Edited in Microsoft PowerPoint to highlight important features of the methodology.

connect variables of water depth, sand grain diameter, flow parameters, ripple formation, symmetry, and spacing. Conclusions addressed wave equations as approximations of the real environment, limiting their solutions to reasonable estimates only.

Hay and Mudge (2005) utilized in situ, rotary acoustic imagery

(Figure 1.4) to assess how energy, versus skewness or asymmetry of incident wave fields is involved in bed state. This study required installment of large frames into the seabed

equipped with rotary sonars to record images of ripple formation. Observations (moving shoreward) included irregular ripples, cross ripples, linear transition ripples, lunate megaripples, and flat bed. Hay and Mudge were able to relate bed state to wave energy, wave skewness, wave period, and sediment grain size, while concluding that the bed state storm cycle evolves independent of previous bed states. Cheel (2007), and Hay and Cheel (2008) employed similar technologies, using fan beam sonar to study cross ripple formation. Cheel explored the mechanisms involved in cross ripple formation by observing the growth and decay of storm bed states for more than 2 months. He was able to demonstrate that the long-crested component of cross ripples occurred in two dominant orientations. Lab experiments were conducted, using a ripple cart with sand and tank and “Scotch Yolk” assembly to generate wave motion to examine how disturbances, such as a pipe inserted in the bed, might affect the formation of cross ripples. The study concluded that cross ripples initiated as small, localized features before extending over the entire bed. Cheel and Hay (2008) examined the directional properties of incident waves and their influence on cross-rippled beds, again using rotary fan beam sonar. It was determined that (1) cross ripples are not a function of wave propagation from two different directions, (2) ripples were independent of prior bed state, and (3) cross ripples are function of hydrodynamic forcing conditions, formed during active transport.

1.3 Thesis Objective: Purpose of the Study

Lunate megaripples and cross ripples are not well studied in the literature and the conditions required for their formation are unclear. Previous surveying methods have recorded observations using instruments installed in the seafloor, which can disturb the sediment and obstruct fluid flow. The main objective of this research project was to refine methodology for observing lunate megaripples and cross ripples non-invasively. The study intended to design a mobile, easily relocated device that could be operated in shallow water, in range of wave conditions, with potential of use in wave conditions that might be of interest to surfers.

A human-powered surface vehicle was constructed as a mount for recording devices, such as a video camera – to record bedform morphologies at varying depths – and sonar – to detect and document ocean floor morphology. Data was collected before, during, and after a storm event to observe the change in bedform geometries and determine flow regime associated with storm conditions. This is the first, simple technology, low cost attempt to collect quantitative data of the seafloor using surface vehicles, and will be considered when assessing whether it will be possible to pursue surficial studies of bedforms. The underlying question addresses what environmental conditions – such as wind speed, wave height, etc. – these bedforms are characteristic of. Knowledge of environmental conditions influencing certain bedform development has been utilized in previous studies to identify beach environments in the geologic record. Evaluating environmental conditions required to form certain bed features may be useful for understanding cross-shore sediment transport and coastal erosion. Thus, it is important to develop a baseline understanding of transport related to geometry of bedforms on the seabed, and/or seabed roughness.

Chapter 2: Geological Setting and Study Site

Data was collected at Crystal Crescent Beach (44° 27' 35.0"N 63° 37' 09.6W), located in Crystal Crescent Beach Provincial Park in Sambro, Nova Scotia, Canada. This site was chosen for (1) its close proximity to Dalhousie University, allowing for convenient access fieldwork, and (2) its clear water, allowing for unobstructed visibility of bedforms on the sea floor. Crystal Crescent is a sandy, topographically simple beach, sloping continuously seaward. The beach is southeast facing with nearby offshore

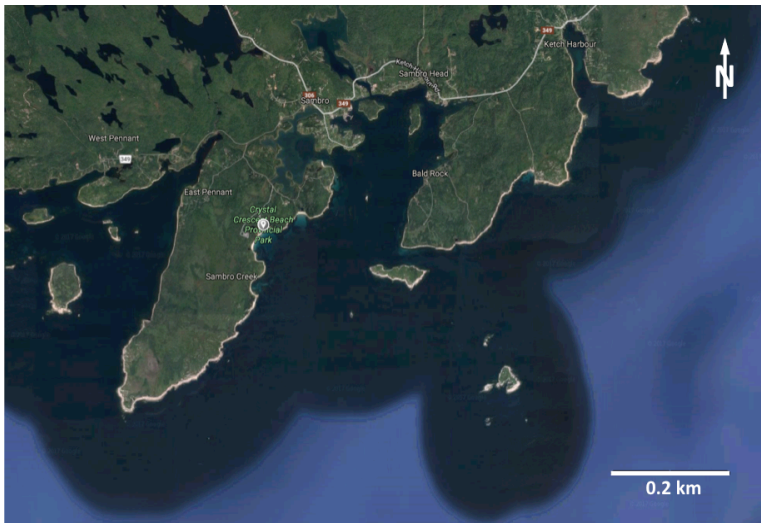


Figure 2.1 Crystal Crescent Beach, its orientation relative to north, and surrounding geographic features including offshore islands.

islands (Figure 2.1). The geology of the area is composed of Harrietsfield leucomonzogranite – a plutonic body involved in the granitic intrusion of the Halifax Pluton (Lackey et al. 2011). Beach sediment derived from nearby boulders is generally composed of

granitic minerals, including quartz, potassium feldspar, micas, and ilmenite. Beach sands also contained small shell fragments and other fragmented organic material such as seaweed. The specific study site was accessed from the parking lot by following the left-most pathway towards the beach (Figure 2.2). Since the park was closed during the fall and winter months, crowds of people were not a hindrance for data collection.

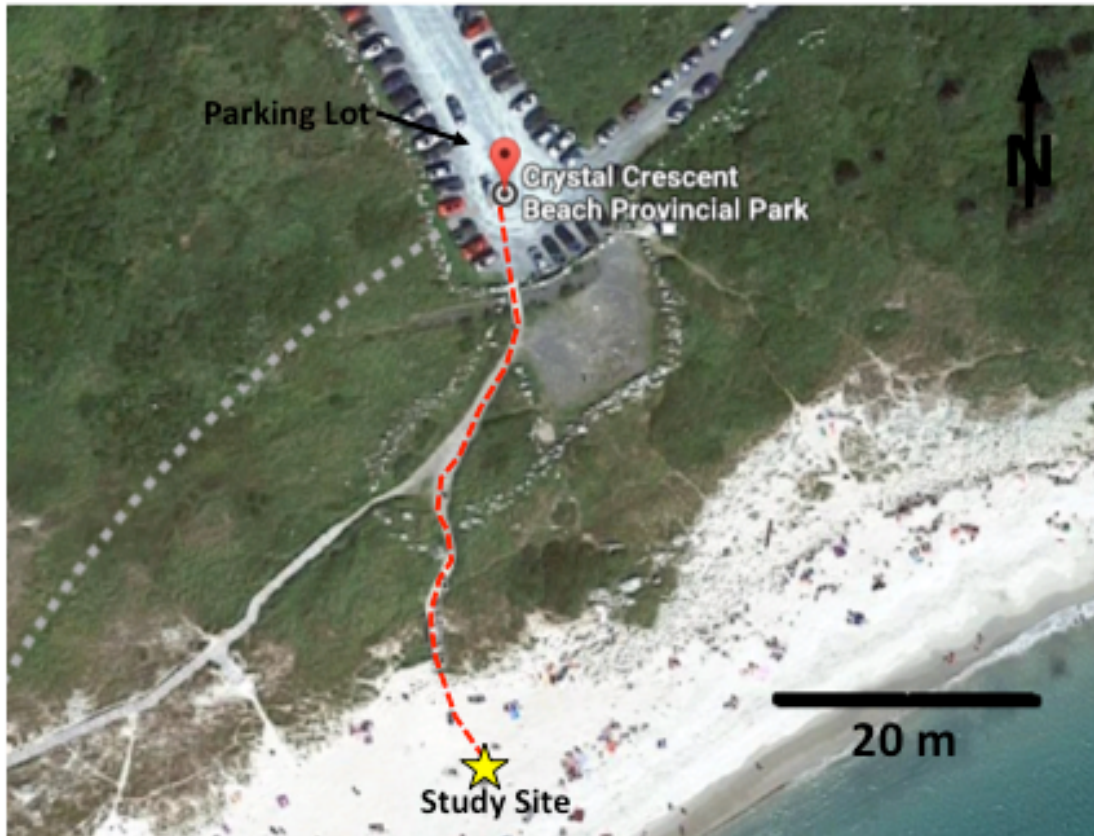


Figure 2.2 Path (red dashed line) from Crystal Crescent Provincial Park parking lot to exact position at the study site (yellow star) where surveying materials were assembled.

Chapter 3: Methodology

3.1 Preparation for Fieldwork

3.1.1 Constructing the Surface Vehicle

A surfboard-surface-vehicle was constructed as a platform for mounting technological devices required to record data in the field (see Section 3.2: Field Technologies and Techniques). Hay and Cheel previously used the surfboard in a study of fluid mud formation and turbulence in the Peticodiac River. It was received for this project complete with three holes cut through the fiberglass and foam, and a framework

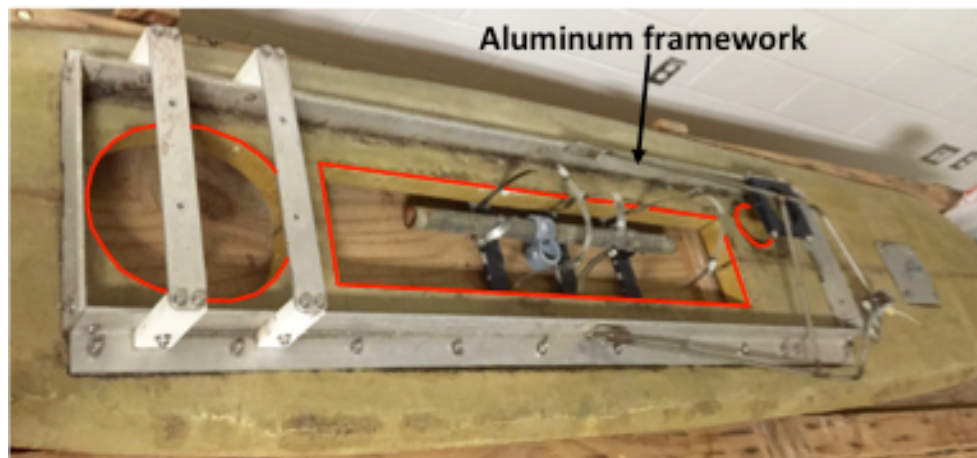


Figure 3.1 State of the surfboard as received. Cut outs indicated by red outline and steel instrumentation (indicated by lack arrow) from the previous project that the board was used in.

of aluminum angle and flatbar for mounting field equipment (Figure 3.1). The aluminum was removed from the board surface and the surface was scrubbed using steel wool, soap and water. Foam exposed in the holes cut into the board was sealed using fiberglass, resin and hardener. Any surficial damages to the board were also repaired in this manner. Repairs were left to dry, then sanded using an electric sander and fine grit sandpaper. The board was taped and painted. Metal rods recycled from previous instrumentation were scrubbed to remove salt weathering using steel wool, soap, and water. Two 2" by 4" cedar skids were added to the underbelly of the surfboard as a base to screw the flatbar to, and to ensure durability and safety of the surfboard. The skids were each cut to a length of $55\frac{6}{8}$ inches using a handsaw, then edges were planed and

finished using Miniwax Polycrylic Protective Finish. The skids were mounted to the base of the surfboard using silicon where drill holes from the previous project lined the rectangular cutout. Once the silicon had dried, the board was flipped over, drill holes in the steel rods were matched to those on the surfboard, and the aluminum flatbar were secured to the board using long screws that extended through the surfboard into the cedar skids (Figure 3.2).



Figure 3.2 Completed surfboard-surface-vehicle, including front view (left) with aluminum flatbar, and back view (right) with cedar skids.

3.1.2 Weather and Wave Condition Data

Weather, wind and wave conditions were assessed frequently to determine appropriate dates for collecting pre-storm and post-storm bedform data. Three websites were primarily consulted to identify a storm event and changing ocean conditions. Windytv (see Table 1 for URL) was used to consider general weather trends (Figure 3.3). The Weather Network’s Marine Forecast for Sambro Harbour Lighthouse, NS was accessed using the URL in Table 1 and provided tidal cycle information, as well as wind and wind gust data, including direction and speed. The National Data Buoy Centre (NOAA) buoy station 44258 (Halifax Harbour) (see Table 1 for URL) was used to attain values for wave height, wave period, atmospheric pressure, and water temperature. According to information provided by these websites, the dates chosen for fieldwork were November 15, 2017 for recording pre-storm bedform geometries, November 17, 2017 to attain ‘during storm’ data, November 22, 2017 for a second attempt at during storm data, and November 26, 2017 to evaluate change in the seabed following the storm event. Figure 3.3 shows the buildup of storm conditions to high speed winds and wave heights on November 18th. This forecast prompted the preliminary field work conducted on November 15th.

Table 1. Websites used to collect weather data for the days prior to, during, and following fieldwork.

Type of Data	Website Name	URL
General weather trends	Windytv	https://www.windytv.com/?rain,89.838,-38.454,3
Temperature, wind direction and speed, wind gust direction and speed	The Weather Network Marine Forecast: Sambro Harbour Lighthouse, NS	https://www.theweathernetwork.com/ca/marine/nova-scotia/sambro-harbour-lighthouse
Wave conditions	NOAA Halifax Harbour Bouy	http://www.smsc.ca/resources/weather/halifax-harbour-buoy

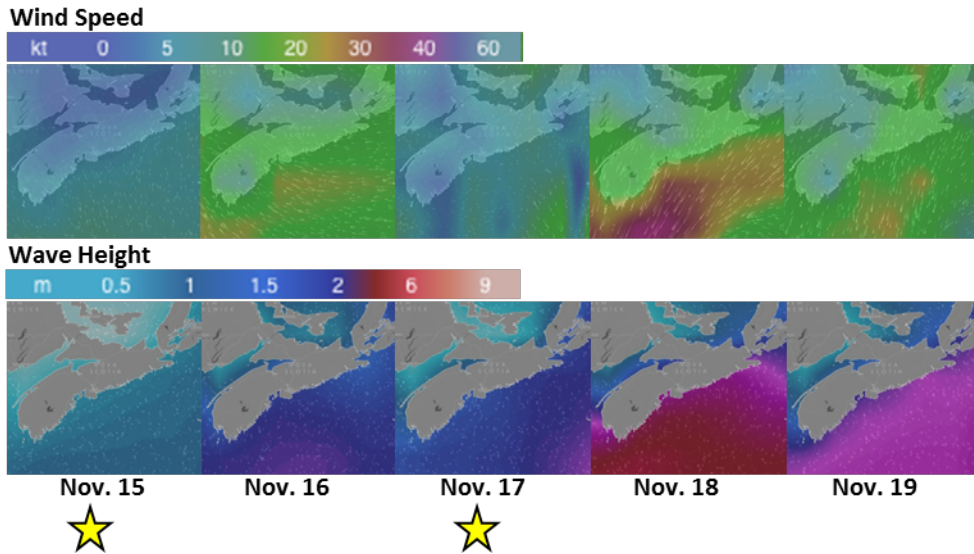


Figure 3.3 Images from WindyTV weather projections showing wind speed (top) and wave height (bottom). Fieldwork was conducted on dates indicated by yellow stars.

3.2 Field Technologies and Techniques

3.2.1 Deeper Fishfinder 3.0 Sonar

The Deeper 3.0 Fishfinder (also referred to as Deeper) is a sonar device used by fishermen to detect seafloor topography, map fishing routes, and detect the presence of fish (Figure 3.4). It requires connection to an android Tablet or cellphone via Bluetooth for GPS coordinates to create a map. In this study, the Deeper 3.0 was utilized to create bathymetric maps of the bed, while tracking the survey path to record cross-shore variation. The Deeper Fishfinder 3.0 application was downloaded to a Samsung Tablet or cell phone prior to fieldwork. It connected to the Deeper 3.0 Fishfinder device upon activation in the field. The settings chosen for data collection were as follows: Smart Imaging – Detailed; Fish icons – off; Frequency – 290Hz; Sensitivity – 100%. The Deeper 3.0 Fishfinder device was tied to the plug at the back of the surfboard-surface-vehicle (where a surf leash would usually be fastened) using fishing twine, which allowed it to float behind the board during fieldwork.



Figure 3.4 Deeper Fishfinder sending out sound waves. Bluetooth is used to connect Deeper to android device to display depth data and profile imaging in real time. Retrieved from <https://www.svb24.com/en/deeper-fishfinder.html>.

3.2.2 GoPro HERO3 Video Camera

A GoPro model HERO3 in a submersible case was utilized to record video images of bedforms on the seafloor (Figure 3.5). The camera was fastened to the surfboard-surface-vehicle using fishing twine. It was mounted on the metal rods in the rectangular “window” of the surfboard-surface-vehicle, pointing down towards the seafloor. Analysis of video imaging allowed for qualitative observations of bedform geometry without causing disturbances at the bed.



Figure 3.5 GoPro Hero3 in submersible case.

3.3 Data Collection and Procedure in the Field

3.3.1 Sand Sampling

Four sand samples were obtained at the Crystal Crescent Beach study site. Samples were intended to represent sediment size at different water depths including (1) onshore, (2) swash zone, (3) 1.5m depth, and (4) 3m depth. Four Ziploc bags were

pre-labeled with the depths listed above using a permanent marker. Upon collection, sand samples were placed in their respective Ziploc bag. The “onshore” sample was obtained at low tide, beneath the high tide wrack line. The “swash zone” sample was obtained onshore in the wave runup. For the 1.5m and 3m depth samples, the Deeper Fishfinder 3.0 and android device were utilized to determine water depth. Then samples were collected from each depth by swimming to the sea floor and placing handfuls of sand into the Ziploc bag. All samples were obtained in early September, when average water temperatures (recorded in Chester, NS) were 16.7°C (World Sea Temperature 2017).

3.3.2 Depth Data and GoPro Video Collection

The surfboard was utilized as a surface vehicle for data collection. Upon arrival at the site, the researcher put on a Ripcurl Flashbomb hooded, chest zip, 5/4 wetsuit, Xcel Drylock TDC round toe 7mm boots, and Xcel Drylock TDC 5-finger 5mm gloves. All field technologies and materials were packed into a backpack, including: fishing twine, often pre-cut to lengths required for fastening field technologies to the board; a Swiss army knife; a Samsung Tablet or Samsung cell phone; watertight dry bag for the Tablet or phone; a transparent submersible box; a GoPro HERO3 and submersible case; the Deeper Fishfinder 3.0; duct tape; and a Rite in Rain notebook with a pencil. Following the park closure on October 10th, 2016, the surfboard and materials were carried from the “Park Closed” gate to the study site outlined in Section 2.0 Geologic Setting and Study Site.

At the study site, environmental conditions were recorded, including: weather – relative temperature, wind, and if it was overcast, cloudy, sunny, etc.; tidal height relative to high tide wrack line; wave height relative to previous field days; exact location of fieldwork; time of day; and observations from time spent in the water. A photograph was taken of the study site for later comparison to other fieldwork days. The board was set up as in Figure 3.6. The transparent submersible case, GoPro HERO3, and Deeper Fishfinder 3.0 were fastened securely to the board using fishing twine. A Samsung cellphone was sealed in a waterproof case and the Deeper Fishfinder 3.0

application on the cellphone was opened. Once the application recognized the Deeper Fishfinder 3.0 device, showing that “Deeper is out of water”, the phone was placed into the transparent submersible case. The case was then closed, and duct tape was utilized to ensure its watertight capabilities.

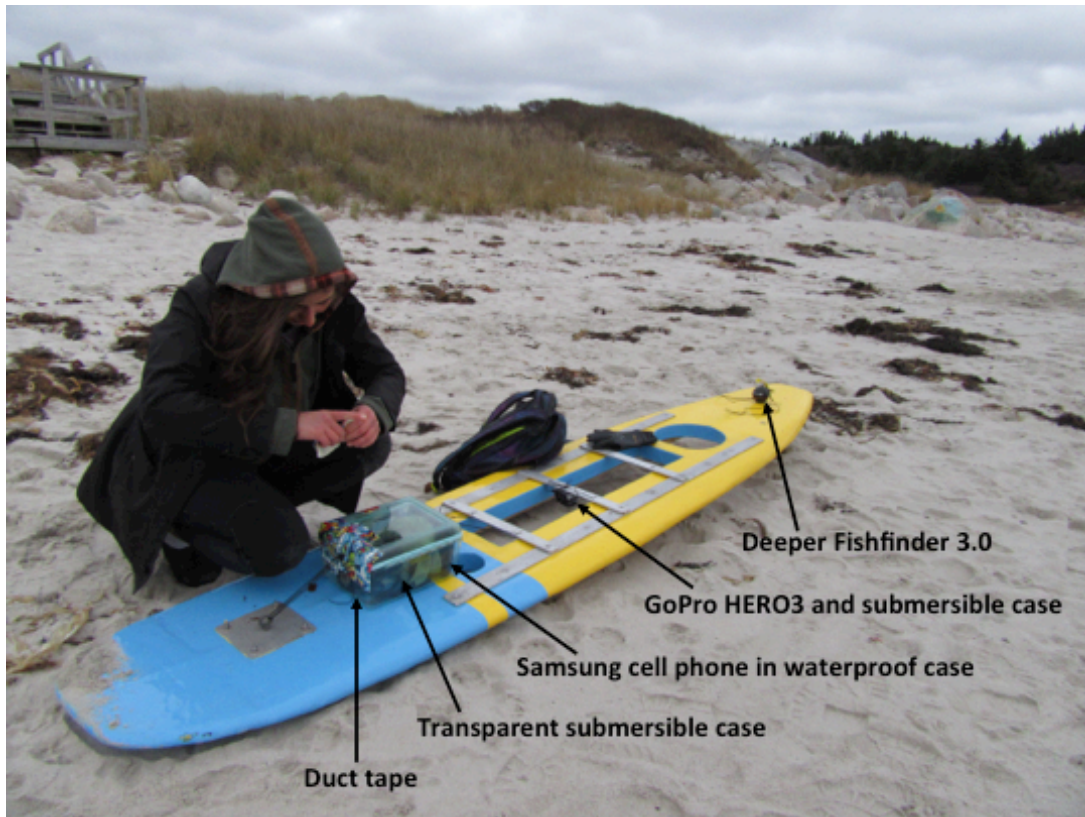


Figure 3.6 Surfboard-surface-vehicle set-up with field materials and technologies (labeled with arrows), including duct tape, transparent submersible case, Samsung cell phone in waterproof case, GoPro HERO3, Deeper Fishfinder 3.0.

The surfboard-surface-vehicle and field technologies were carried to the shoreline where the water was entered. The researcher lay on top of the board and paddled it towards the open ocean, approximately perpendicular to the shoreline, until reaching a depth of greater than or equal to 3m as indicated by the Deeper Fishfinder application on the Samsung cellphone. Then the researcher turned the board towards shore and paddled in, again approximately perpendicular to shoreline. This process was repeated to collect depth, latitude, and longitude data, as well as video images for the ocean floor at the study site.

Paper signs encased in Ziploc bags, then eventually hand signals were used to indicate depth and travel direction towards or away from shore in the GoPro video. For depth, a number of fingers were used to signify number of meters. For example, if the Deeper Fishfinder application on the Samsung cellphone read 2m depth, two fingers were held in front of the GoPro camera lens. Travel direction was defined as out from shore with a fist, and into shore with a flat, open hand. These symbols were incredibly important in later analysis of GoPro videos. Figure 3.7 shows a collection of images from fieldwork procedures.

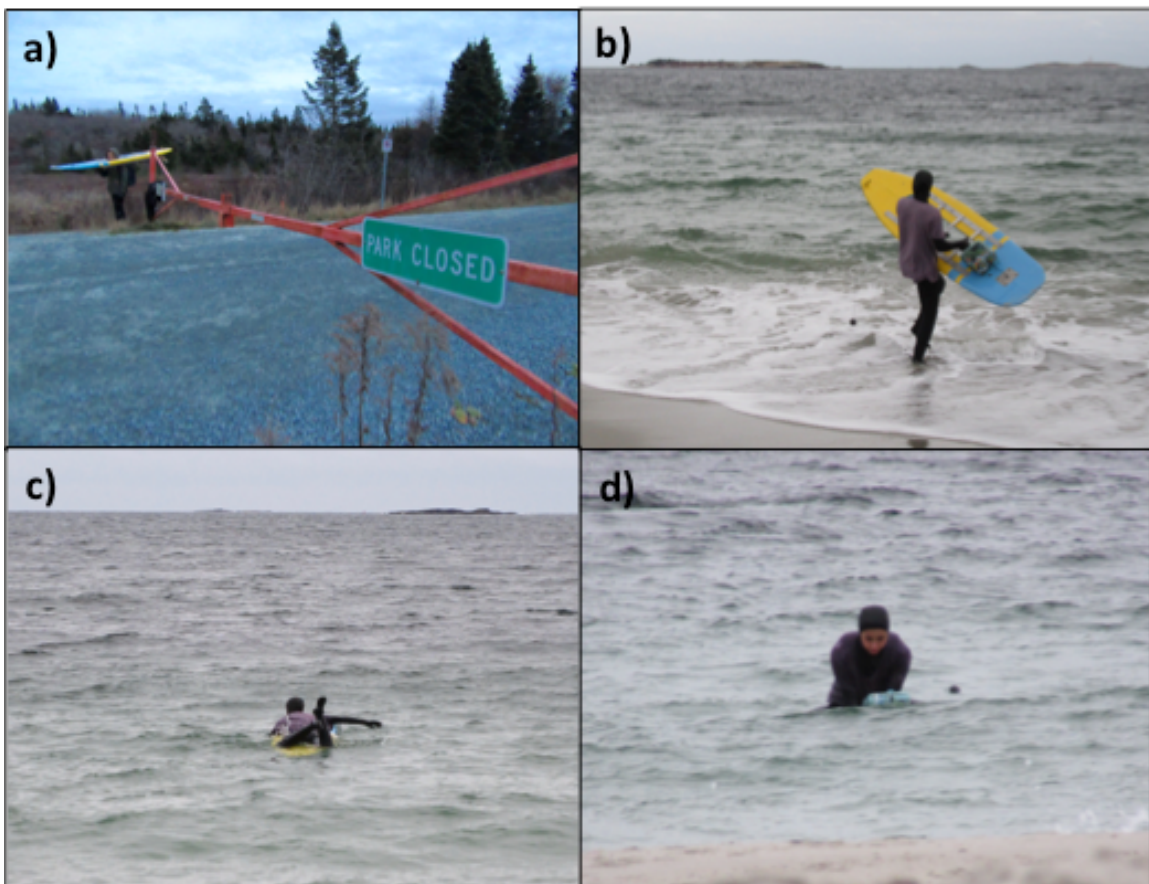


Figure 3.7 A collection of photos showing various field procedures, including: a) passing “Park Closed” sign and gate, researcher equipped with surfboard-surface-vehicle and backpack carrying research technologies and materials; b) walking the surfboard-surface-vehicle, equipped with field technologies, into the water; c) paddling out towards the open ocean; d) observing Deeper Fishfinder 3.0 depth measurement to inform the GoPro video while paddling in towards the shore.

3.4 Data Analysis Methods

3.4.1 Weather Data Analysis

Weather records were accessed from Government of Canada Fisheries and Oceans website <http://www.meds-sdmm.dfo-mpo.gc.ca/isdm-gdsi/waves-vagues/data-donnees/index-eng.asp>. Hourly data from NOAA buoy C44137: East Scotian Shelf between the dates of November 13, 2017 and November 26, 2017 was utilized for analysis. Data from NOAA buoy C44258: Halifax Harbour, the buoy used for fieldwork, was unavailable. Weather data was analyzed using Microsoft Excel to create representative figures (Section 4.0: Results). Variables such as characteristic significant wave height (m), horizontal wind speed (m/s), direction from which the wind is blowing ($^{\circ}$ True North), dry bulb temperature ($^{\circ}$ C), sea surface temperature ($^{\circ}$ C), and atmospheric pressure at sea level (mbar), were compared to determine possible correlation to bedform geometries observed in the field.

3.4.2 Sand Sample Preparation and Sieving

Following collection, samples were taken to the lab where the contents of each Ziploc bag were washed separately to remove the salt. Sand was placed in a beaker and flooded with distilled water, then swirled. Salty water was poured off. This process was



Figure 3.8 Sand samples obtained from varying water depths including: onshore; swash zone; 1.5m; and 3m. Samples were washed and left to dry in aluminum pie tins lined with coffee filters in preparation for sieving.

repeated three times. Washed samples were placed in aluminum pie tins labeled with sample depth and lined with coffee filters (Figure 3.8). Samples were allowed to dry for approximately one week.

The dry samples were weighed, then transferred to a stack of woven wire mesh sieves and placed into a mechanical Ro-Tap shaker, which ran for 15 minutes.

Each individual grain size bin was analyzed for mineralogical composition before being weighed. Each sample was returned to its Ziploc bag.

3.4.3 GoPro HERO3 Video Analysis

GoPro videos collected during fieldwork were carefully analyzed in Final Cut Pro. Each video was imported to Final Cut Pro and opened in “timeline” by selecting “Clip”, then “Open in Timeline” from the dropdown menu. Shadows were darkened to make bedforms more identifiable using the “Colour Board” to adjust the Exposure and Saturation. Still frames were extracted at depths of 1m, 1.5m, 2m, 2.5m, 3m, 3.5m, and 4m to show representative, as well as uncharacteristic bedforms and features at each depth. Stills were extracted using the “Share” option, then selecting “Extract Current Frame”. Each still frame was then imported into iPhoto, where it was further enhanced using the “Adjust” feature to move the Brightness, Contrast, Shadows, and Black Point settings to accentuate ripple forms. Figure 3.9 shows the effect of each adjustment on the photos.

For a complete list of enhancements for each still frame extracted, see Appendix B.

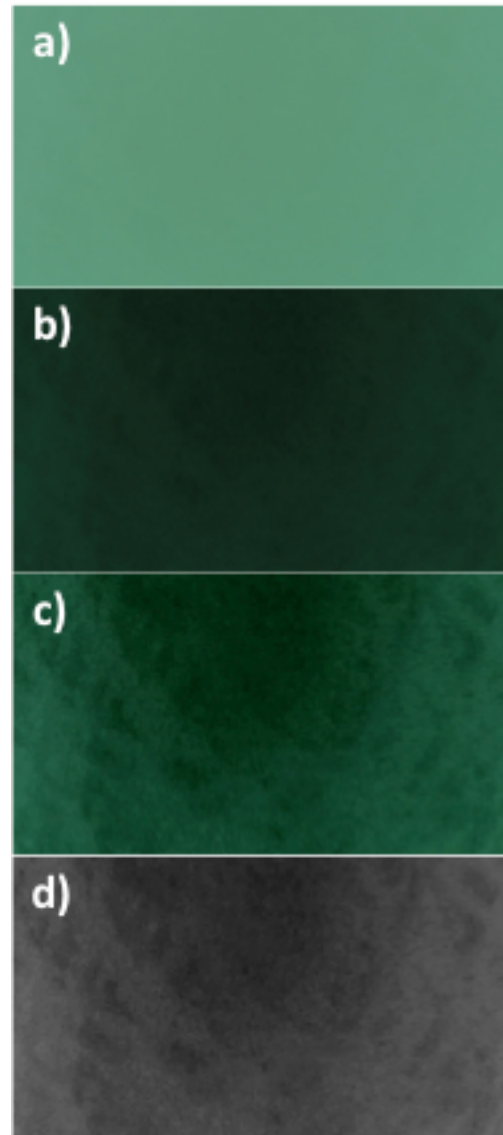


Figure 3.9 Sample of bedform still frame from GoPro video recorded on Nov. 17, 2017. Photo a) shows the video completely unedited, b) shows Exposure and Saturation adjustments made in Final Cut Pro, c) shows final enhancements made in iPhoto to increase contrasts, and d) illustrates the undistorted photo from Matlab.

In order to calculate a proper scale, the fisheye effect of the GoPro camera lens was removed by calibrating the camera in the lab using Camera Calibration Toolbox for Matlab (http://www.vision.caltech.edu/bouguetj/calib_doc/). Videos of a checkerboard pattern were obtained in a large tank filled with water. The checkerboard was

comprised of a paper print out of black and white square checkers sealed between two sheets of acrylic. With the camera held steady at one end of the tank, the checkerboard was moved about at the opposite end of the tank so as to acquire images at various different angles (Figure 3.10). Videos were then imported to Final Cut Pro where specific still frames of each checkerboard orientation were extracted using the “Save Current Frame” function. These images were uploaded to Matlab and lens-distortion parameters estimated using the Camera Calibration Toolbox (Figure 3.10).

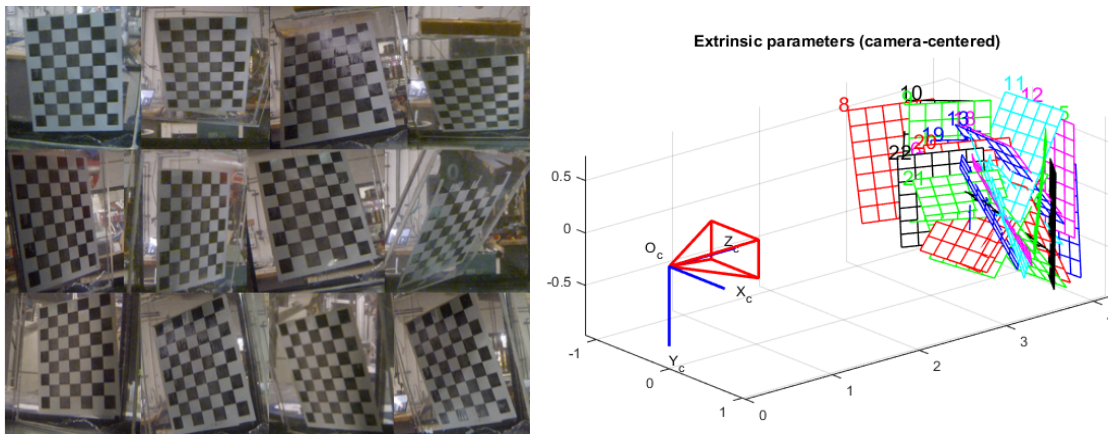


Figure 3.10 (Left) Examples of video images of a checkerboard held in different orientations, used in the procedure for calibrating the GoPro Hero3 camera to remove fisheye. (Right) Diagram of extrinsic parameters of GoPro camera lens generated by Matlab. The red pyramid indicates the position of the camera in the tank, while the grids indicate various orientations of the checkerboard.

Scale was then calculated using an undistorted image of a wetsuit boot of known size (12.4 cm) and comparing its length to the image pixels. Figure 3.11 shows that 200 pixels is equal to 12.4 cm. This information was then applied to all other images to evaluate the scale of the observed bedforms.

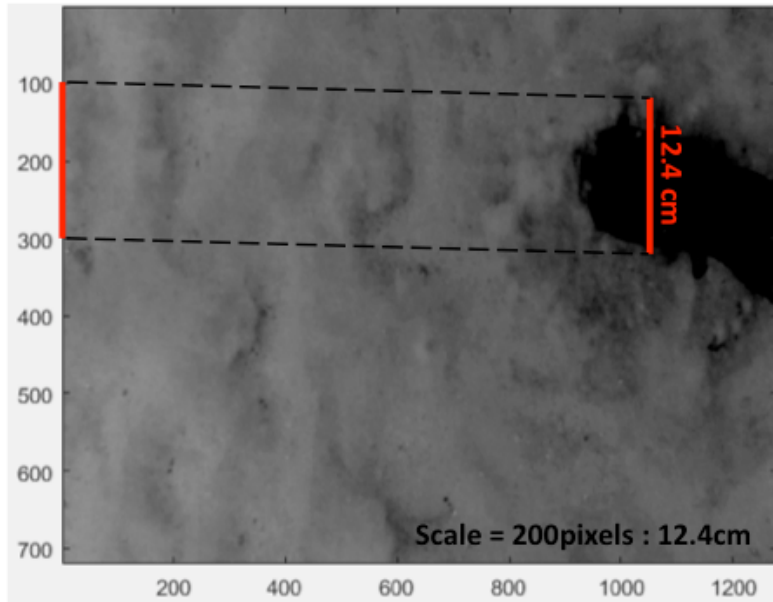


Figure 3.11 Representation of how scale was calculated for extracted GoPro stills. The width of a wetsuit boot (black object) measured to be 12.4cm is equal to 200 pixels in the photo.

3.4.4 Deeper Fishfinder 3.0 Data Analysis

Data recorded by the Deeper Fishfinder 3.0 sonar device was analyzed using Matlab. Multiple figures were produced for each day of fieldwork, including: (1) the traverse path, created by graphing longitude versus latitude; (2) a scatter plot coloured according to depth to show topographic change along the traverse; and (3) three-dimensional bathymetric map, constructed using latitude and longitude data with depth data to show seafloor geometry. The traverse paths were constructed by comparing latitude (y-axis) and longitude (x-axis) of the data points collected on each day. The three-dimensional bathymetric map compared latitude (y-axis) and longitude (x-axis) of each data point with depth (z-axis) to construct a representation of seafloor topography. The graphs were used to compare swimming path travelled on each day with change in depth data and bathymetry throughout the storm event.

Chapter 4: Results

4.1 Weather and Sea Conditions

Through comparison of characteristic significant wave height (m), horizontal wind speed (m/s), direction from which the wind is blowing ($^{\circ}$ True North), dry bulb temperature ($^{\circ}$ C), sea surface temperature ($^{\circ}$ C), and atmospheric pressure at sea level (mbar), the following relationships were observed. Characteristic significant wave height – also referred to as wave height – prior to fieldwork on November 13th was approximately 5m. These conditions might offer an explanation for the isolated cross ripples observed in video images of bedforms from “pre-storm” November 15th. As expected, wave conditions on November 15th show significantly smaller wave height, averaging at 1.1m throughout the day. Wave heights between November 17th and November 25th suggest two storm events – the first with wave heights of up to 8m, and the second with wave heights of up to 12m. This data was consistent with observations in the field, as wave heights on November 22nd were greater than November 17th. Wave height was relatable to horizontal wind speed trends, as peak wind speed magnitudes generally corresponded to larger wave height events (Figure 4.1). Average wave heights on each day of fieldwork outlined in Table 2.

Table 2. Average of hourly wave heights for each day of fieldwork, reported by NOAA buoy C44137.

Date	Description	Average Wave Height (m)	Peak Wave Height (m)
November 15, 2017	Pre-storm	1.1	1.42
November 17, 2017	During storm (1)	1.8	2.24
November 22, 2017	During storm (2)	4.0	4.54
November 26, 2017	Post-storm	1.0	1.21

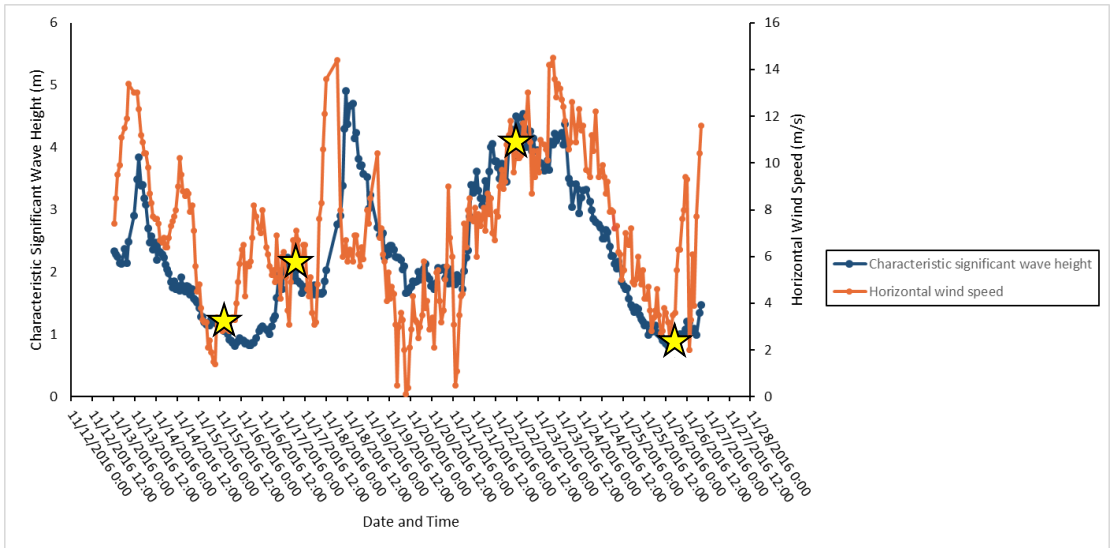


Figure 5 Comparison of characteristic significant wave height on the primary y-axis (blue) and horizontal wind speed on the secondary y-axis (orange). Yellow stars indicating conditions on days where fieldwork was conducted.

Direction from which the wind is blowing ($^{\circ}$ True North) showed a general relationship to horizontal wind speed (Figure 4.2). For example, peak wind speed magnitudes corresponded with winds blowing from approximately $250\text{--}290^{\circ}$ (West), with the exception of one instance on November 7th and 8th where high-speed winds were blowing from $40\text{--}60^{\circ}$ (approximately NE).

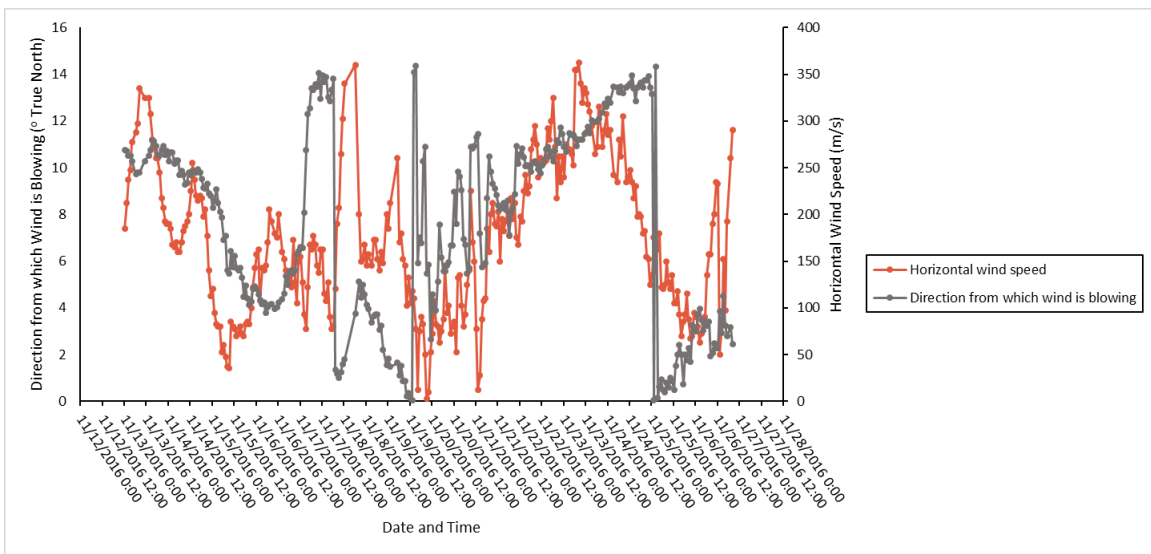


Figure 4.2 Comparison of direction from which the wind is blowing on the primary y-axis (gray) and horizontal wind speed on the secondary y-axis (orange).

Atmospheric pressure at sea level is related to horizontal wind speed and wave height such that high-pressure events lag slightly behind circumstances of high wind speed/larger wave height (Figure 4.3). Periods of highest wind speed are generally associated with low-pressure atmospheric conditions. Other, less notable relationships showed dry bulb temperature and wind speed showed weak relationships, with temperatures generally decreasing during episodes of high magnitude wind speed. Atmospheric pressure and wave height showed a relationship where peak wave heights generally followed low-pressure events.

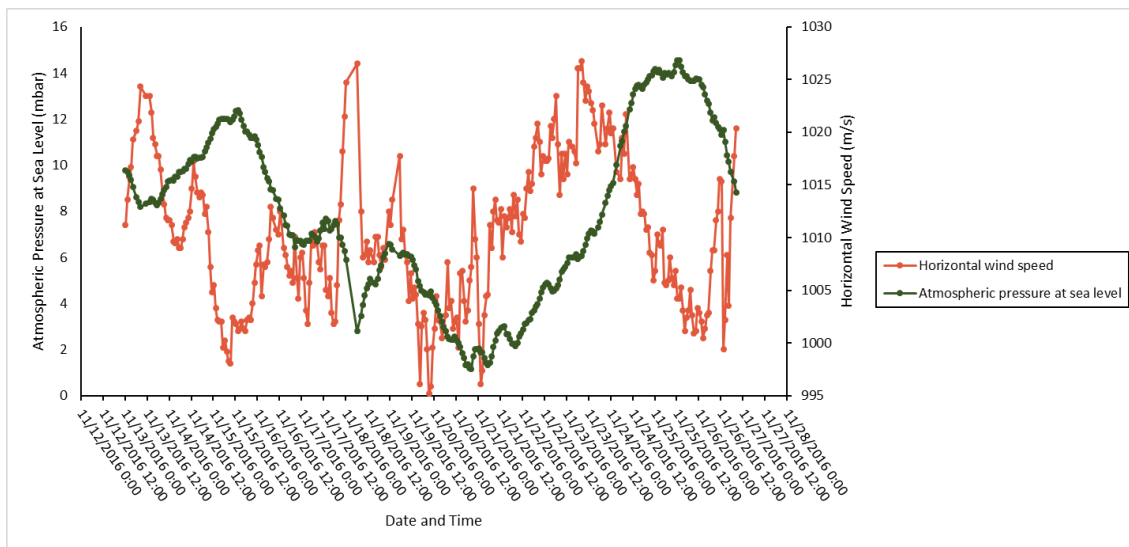


Figure 4.3 Comparison atmospheric pressure at sea level y-axis (gray) and horizontal wind speed on the secondary y-axis (orange).

4.2 Grain Size

All samples were composed of high percentages of quartz, with potassium feldspars and micas appearing in grain sizes of 600 μ m and smaller. Each sample displayed varying distributions of grain size with a general tendency towards finer grains with increasing depth. Sediment sampled from each depth displayed non-symmetric distributions, a mean, median, and mode of the samples are three different values.

The histogram of the sample collected from onshore was skewed towards small grain sizes, which a coarse tail at the largest grain size (grain diameters of greater than

1.18mm). The most frequently occurring grain size from this location was 300 μ m. A significant quantity of sand sampled from the swash zone was greater than 1.18mm, including gravel-sized grains up to 3cm in diameter. Sediment from this location was very smooth and rounded. Coarse to very fine-grained sand existed here as well, but modal grain size occurred in the 1.18mm sieve. Sediment from 1.5m depths was generally skewed towards medium to very fine-grained sand, with a modal grain size of 300 μ m. The “coarse tail” in the grain size distribution indicates captured particles from the foreshore. Sand sampled from 3m depths is uniformly medium to very fine-grained sand, with 250 μ m as the most frequently occurring grain diameter. See Figure 4.4 for a grain size distributions and representative photos of sediment from each location.

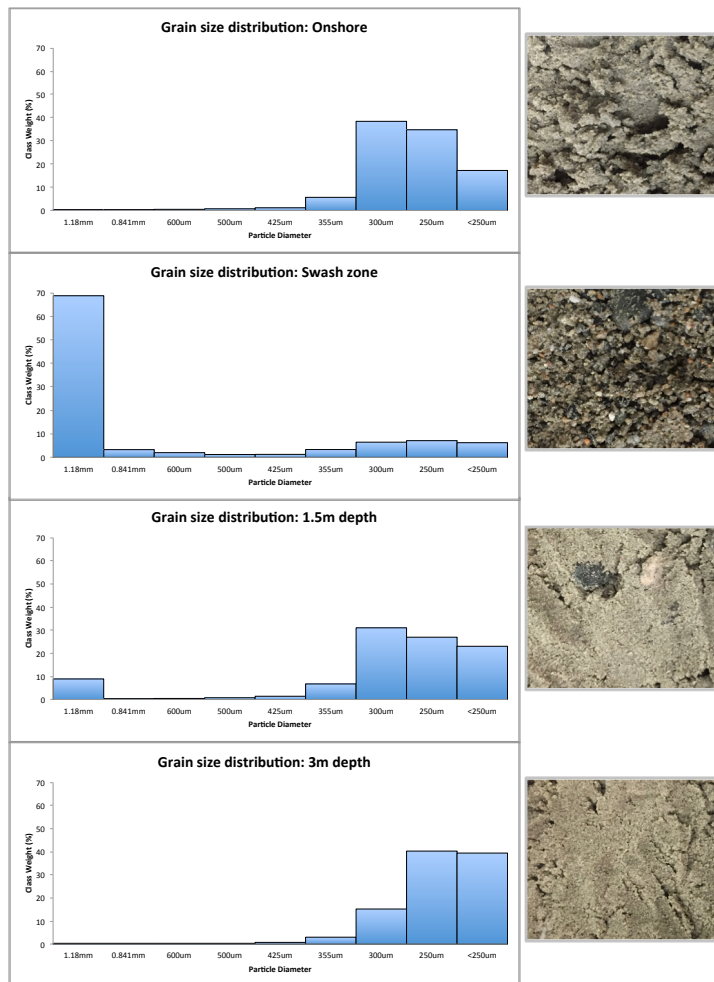


Figure 4.4 Grain size distribution histograms (left) and photos (right) of samples from onshore, swash zone, 1.5 m depth, and 3 m depth. Blue bars indicate percent weight of sand in each sieve size.

4.3 Deeper 3.0 Fishfinder Data

Figure 4.5 shows the path travelled during the traverse on each day of fieldwork. Figure 4.5(1) is the path travelled on November 15, 2017. The line nearer to the number '1' shows where the water was entered, while the line nearer to the top left corner of the figure indicates where the water was exited. The location of the beach was normal to these two lines (see Figure 4.6). Figure 4.5(2) is the path travelled on November 17, 2017. The path shows less consistency in length of switchbacks due to larger wave conditions. Figure 4.5(3) is the path travelled on November 22, 2017. This path is very inconsistent and seemingly random. Extremely large wave conditions with waves breaking onshore made it difficult to swim any direct path. Figure 4.5(4) is the path travelled on November 26, 2017. Calmer weather and wave conditions allowed for a more complete survey of the seafloor.

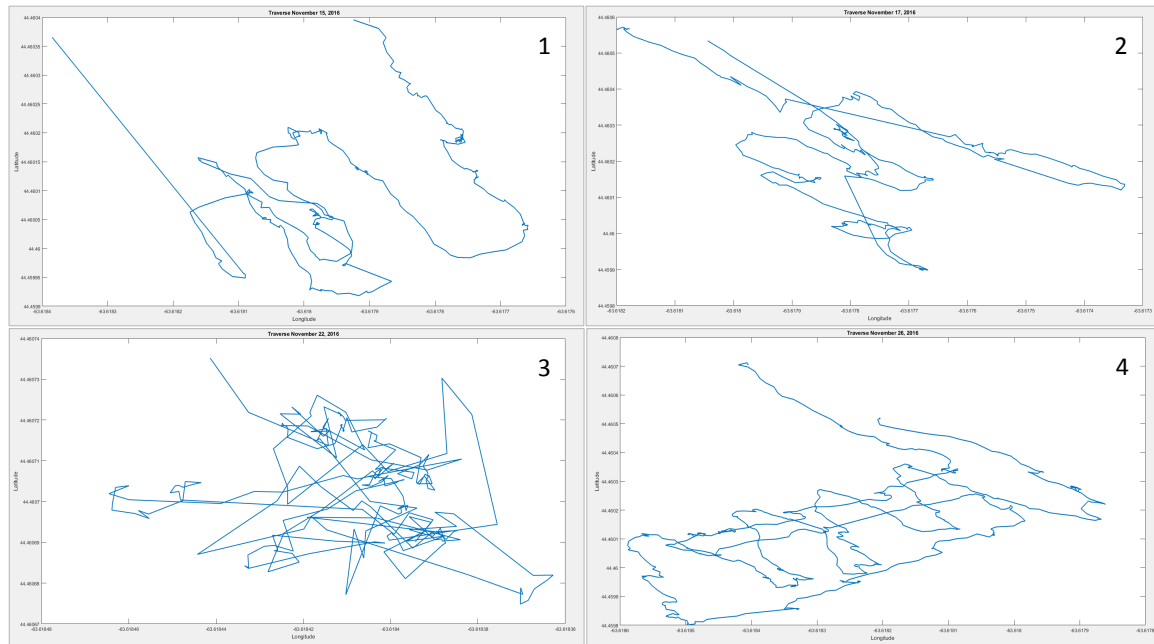


Figure 4.5 Traverse paths during each survey. Latitude is shown on the y-axis, Longitude is shown on the x-axis. (1) Traverse path recorded on pre-storm November 15, 2017. (2) Traverse path recorded during storm on November 17, 2017. (3) Traverse path recorded during storm on November 22, 2017. (4) Traverse path recorded post-storm on November 26, 2017.

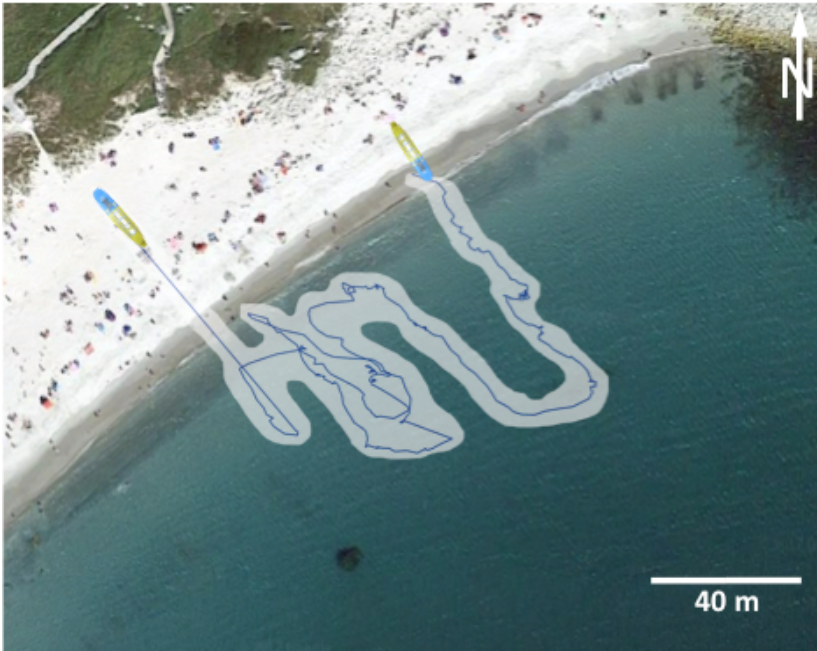


Figure 4.6 Swim path from November 15, 2017 superimposed on Google Earth image of the study site at Crystal Crescent Beach. Placement of the path is an approximation to be used for reference.

Figures 4.7, 4.8, and 4.9 illustrate change in depth along the traverse (top), compared to a representation of bathymetry (bottom). Depth is displayed as metres below sea level in a legend on the left side of each figure. Values range from 0m to greater than 7m depth. In Figure 4.7 from November 15, 2017, the beach profile slopes continuously seaward, deepening gradually. Figure 4.8 from November 17, 2017, shows a more rapid depth increase in comparison. Data from this day appears more convoluted, with data points at 3.5–5m depth overlapping with data points reading 1–2m depth. Post-storm, Figure 4.9 from November 26, 2017 shows a more consistent gradient, which is comparable to pre-storm Figure 4.7. No figures are provided for November 22, 2017, as the sonar did not record depth data on this day.

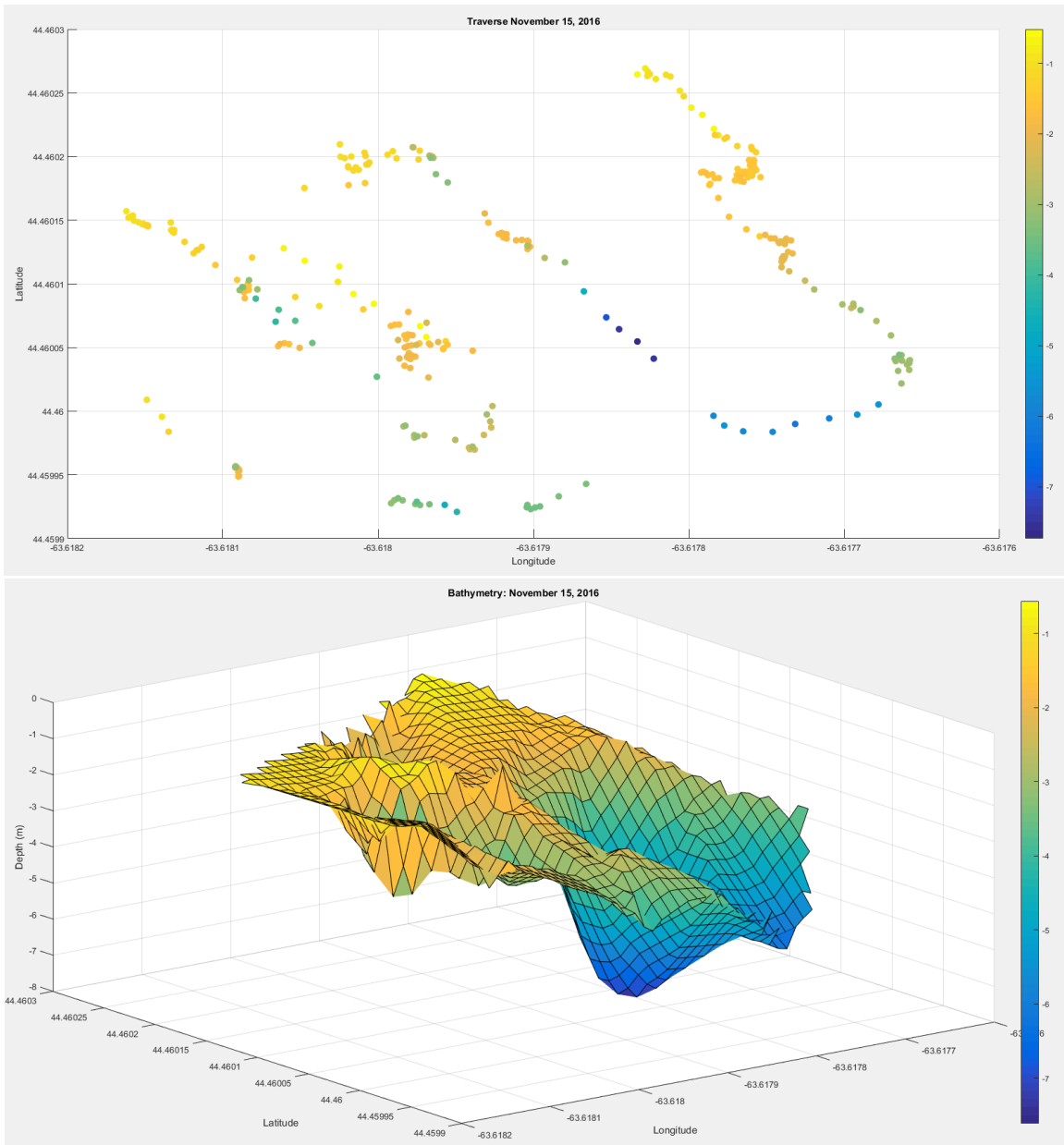


Figure 4.7 Depth in metres along traverse path (top), compared to three-dimensional representation (bottom) of bathymetry on November 15, 2017. Longitude plotted on x-axis, latitude plotted on y-axis, depth plotted on z-axis.

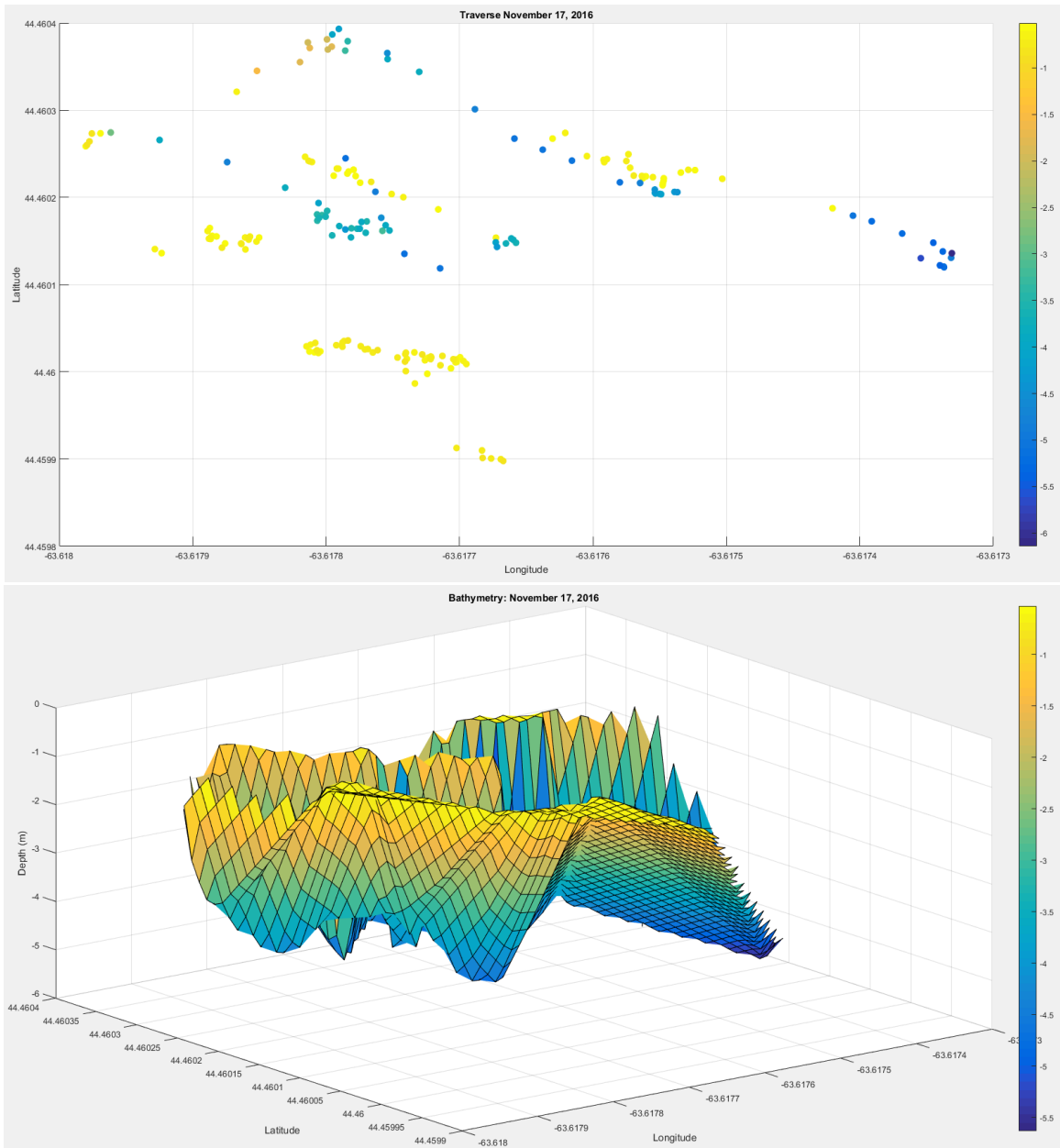


Figure 4.8 Depth in metres along traverse path (top), compared to three-dimensional representation (bottom) of bathymetry on November 17, 2017. Longitude plotted on x-axis, latitude plotted on y-axis, depth plotted on z-axis.

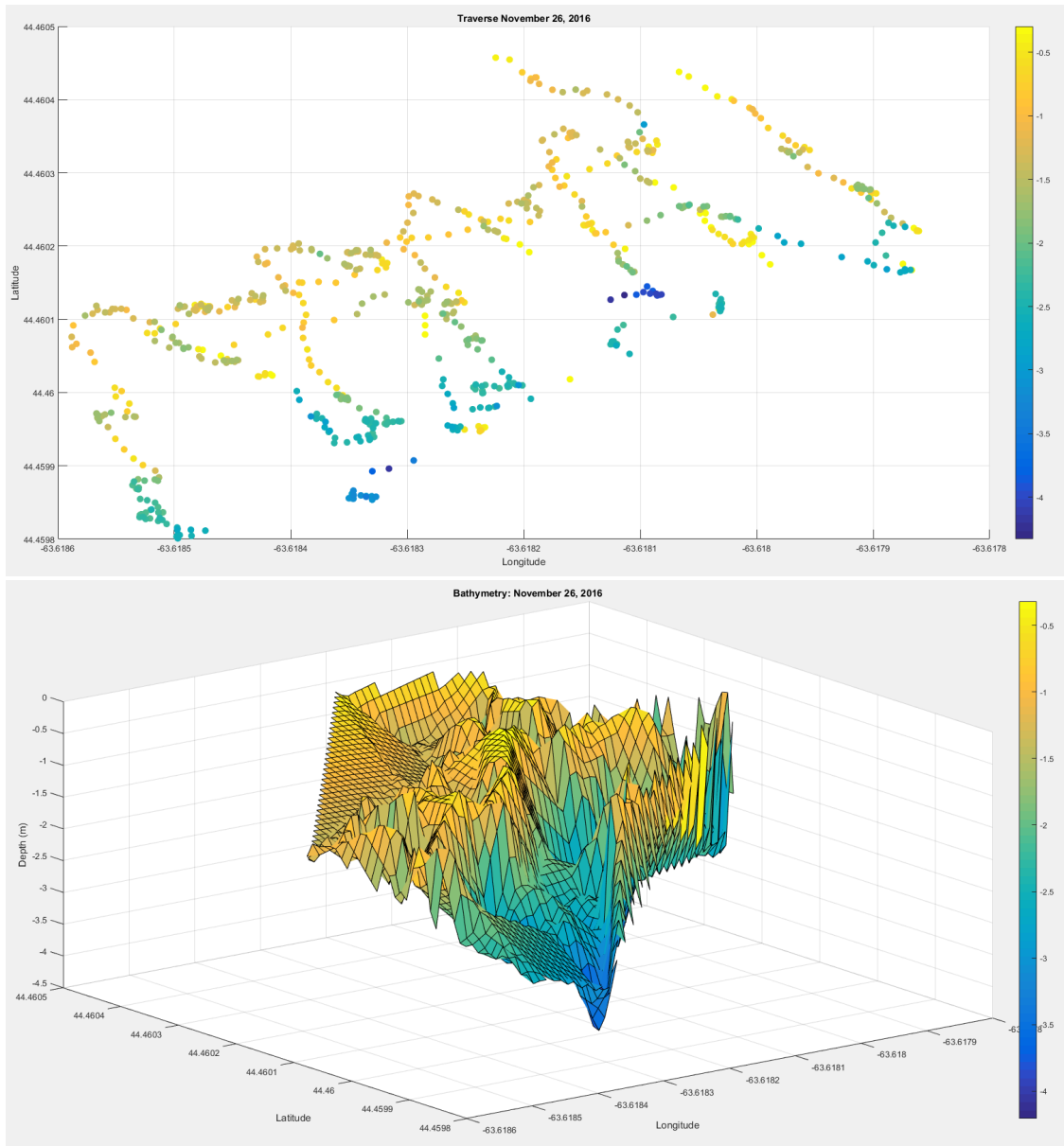


Figure 4.9 Depth in metres along traverse path (top), compared to three-dimensional representation (bottom) of bathymetry on November 26, 2017. Longitude plotted on x-axis, latitude plotted on y-axis, depth plotted on z-axis.

Figure 4.10 shows the transformation of the seafloor from before the storm on November 15 (1), to during the storm on November 17 (2), to after the storm on November 26 (3). Again, no figures are provided for November 22, 2017, as the sonar did not record depth data on this day. The shoreline for these figures is the same as for Figures 4.7–4.9 above. Depth measurements from before the storm are comparable to measurements following the storm. Distinct features appear relatively similar, for example, the dark blue circle indicating 6–7m depth, and turquoise trough to the right

of it. These features in the figure from November 26 are shifted to the left of their location on November 15. The Figure 4.10(2) from during the storm on November 17 shows more complex bathymetry that differs dramatically from Figure 4.10(1) and (3). Blue troughs are observed, indicating deeper waters extending to the shoreline.

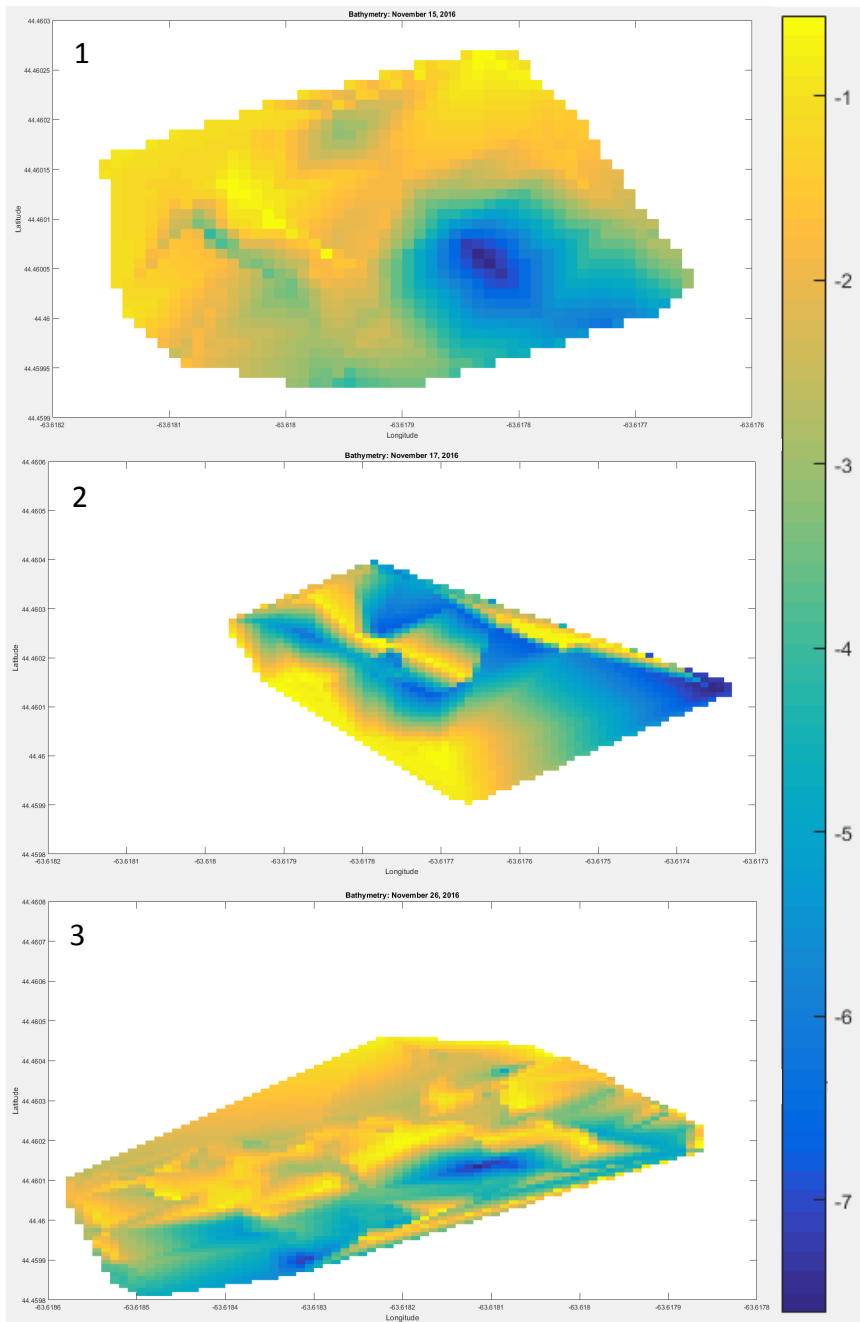


Figure 4.10 Flattened representation of the seafloor depth, showing the change occurring from before the storm on November 15, 2017 (1), to during the storm on November 17, 2017 (2), and then following the storm on November 26, 2017 (3). Longitude plotted on x-axis, latitude plotted on y-axis.

4.4 GoPro Videos: Observations and Images

GoPro videos showed that ripples generally became straighter and more continuous with increasing depth. Ripple geometries between depths of 1m–5m changed dramatically from their shapes before the storm event. Specific descriptions of ripples at 1m, 2m, and 3m depths are given below. Sand was observed to mobilize due to wave energy and regularly suspended above the bed at a depth of 2m. This was also the depth where cross ripple formation occurred during the storm event. In the GoPro videos, suspended sand was observed to move quickly in a shoreward direction then remain suspended in place momentarily before rapidly changing directions and flowing seaward. The shoreward motion of sediment was much more intense than the seaward movement. Suspended sediment and vegetation closer to the surface appeared to move quickly towards the shoreline before sand at the bed was mobilized, as if lagging behind particles closer to the surface. GoPro videos could not capture seafloor bed states of the seafloor during peak wave heights on November 26, 2017 due to large quantities of bubbles and suspended sediment in the water column.

Ripples recorded on November 15, 2017, prior to the storm event, at depths of 1m resembled small, three-dimensional (3D), somewhat lunate forms with coarser sediment in their troughs (Figure 4.11). The seafloor at 1m became almost planar towards the shoreline where wave energy increased (Figure 4.12). Closer to 1.5m, ripples maintained the same 3D form, but coarse sediment was not present (Figure 4.13). During the storm event November 17, 2017, ripples at 1m depth appeared as continuous, sigmoidal ripples with short wavelengths (no image available), while ripples between 1–1.5m resembled irregular cross ripples forming around obstacles on the bed (Figure 4.14). There were considerable quantities of suspended sediment, including pieces of seaweed (up to 1m long) in the 1-1.5m depth zone, but little to no coarse sediment, as before the storm (Figure 4.15). Following the storm on Nov. 26, 2017, ripples between 1 – 1.5m resembled domes and depressions with pockets of coarse (pebble sized) sediment in troughs, as well as small scale (approximately 15cm across) lunate ripples (Figure 4.16).

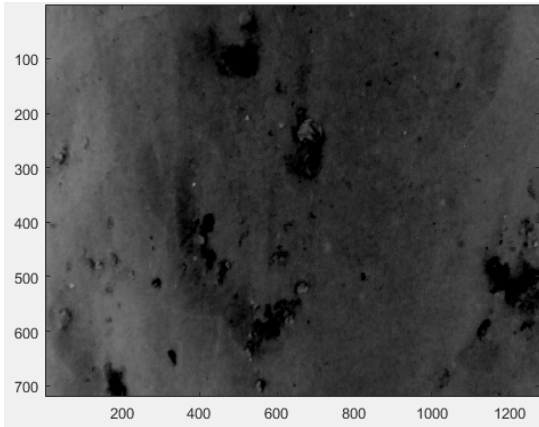


Figure 4.11 Photo from Nov. 15: 1m depth. Somewhat lunate ripples with coarse-grained (pebble sized) sediment in the troughs.

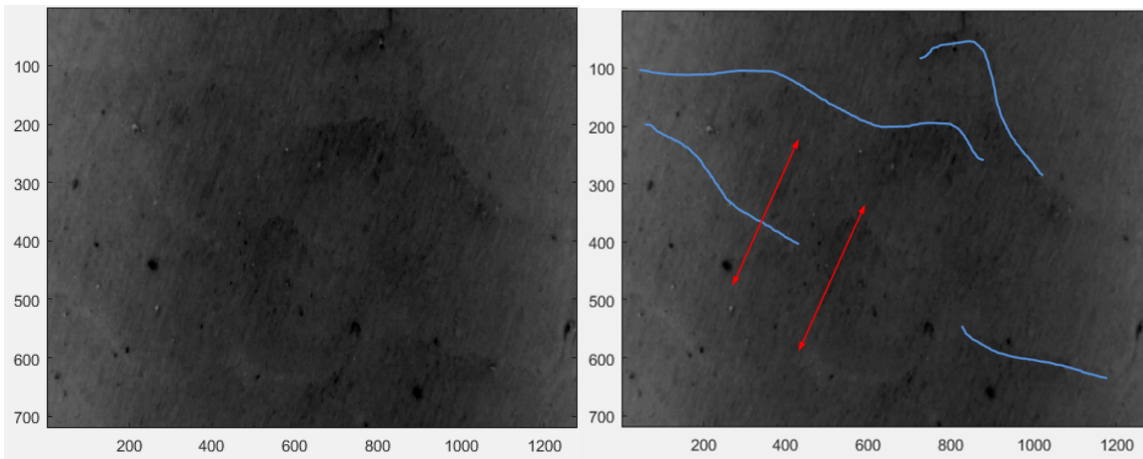


Figure 4.12 Photo from Nov. 15: 1m depth. Relatively low amplitude (flat) ripples (indicated by blue lines), crossed by thin linear structures oriented perpendicular to shore (indicated by red line).

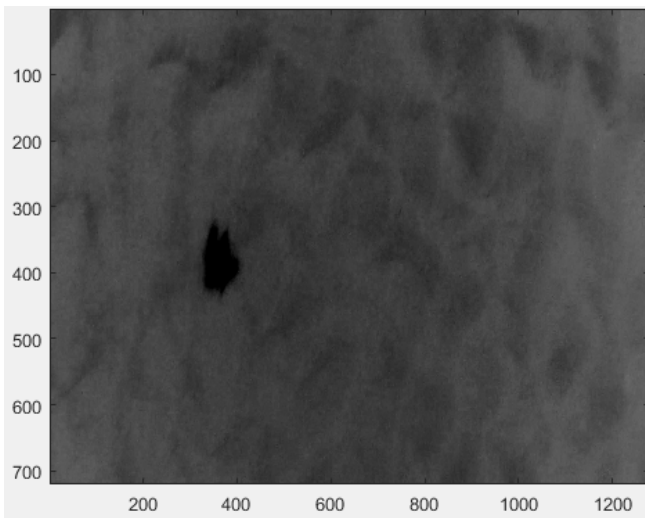


Figure 4.13 Photo from Nov. 15: 1.5m depth. Complex, three-dimensional ripples without coarse sediment in the troughs. Black irregularly shaped object is a small plant in the seabed.

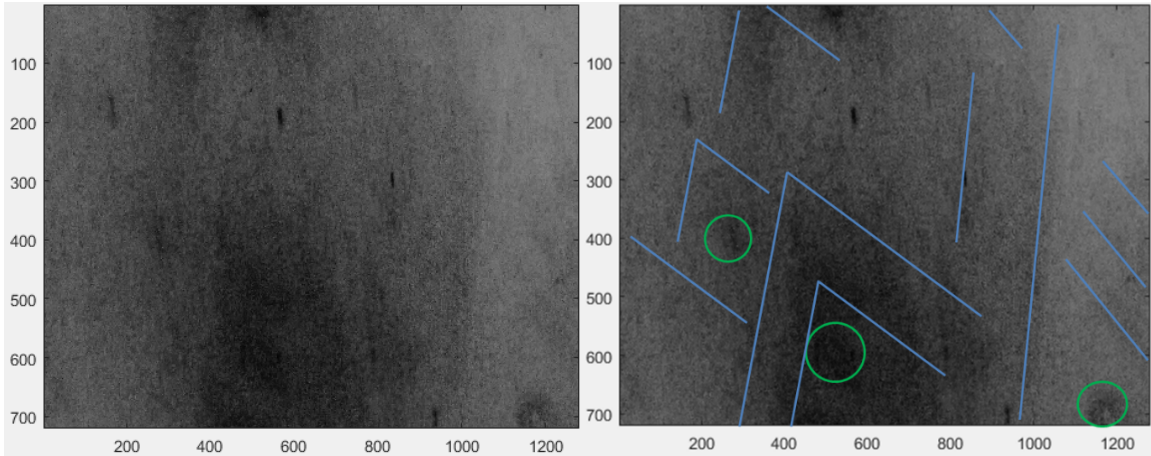


Figure 4.14 Photo from Nov. 17: 1m depth. Multiple small plants in the seabed (indicated by green circles) surrounded by complex crossing of bedforms and irregular cross ripples (troughs indicated in blue).

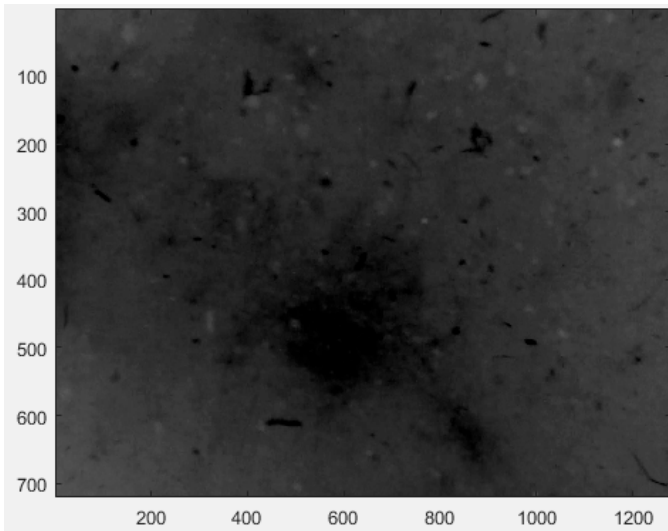


Figure 4.15 Photo from Nov. 17: 1m depth, showing highly turbid water at 1m near the swash zone, with considerable quantities of suspended sediment and large seaweed pieces.

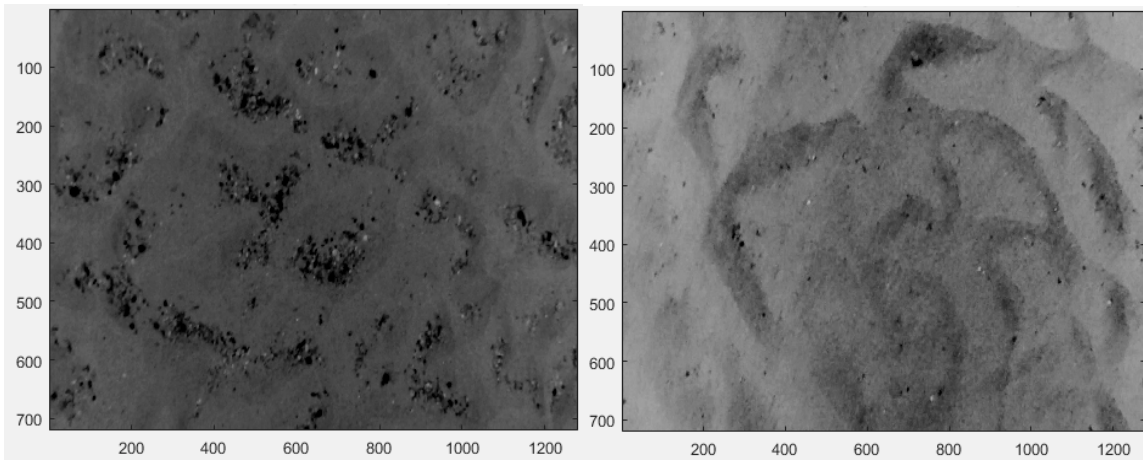


Figure 4.16 Photo from Nov. 26: 1.5m depth. (Left) 'Domes and depressions' with coarse grained (pebble sized) sediment in their troughs. (Right) Small scale lunate ripples.

At depths of 2m, pre-storm ripples had diverse geometries including tighter, sharper 3D forms than at 1m depth, “flower-like” structures, and isolated, discontinuous cross ripples (Figure 4.17). At 2.5m, ripple crests become lengthened and more continuous (Figure 4.18). During the storm, ripples at 2m depths transformed into regularly spaced cross-ripples showing long, straight, continuous crests with smaller crests in their troughs. The long, continuous ripples intersected each other at approximately 60° angles, forming larger scale diamond shapes. Diamond points seemed to centre around, and propagate shoreward from obstacles in the bed (Figure 4.19). Following the storm, ripples took on regular, more elongate, sinusoidal, continuous forms with isolated cross ripples (Figure 4.20).

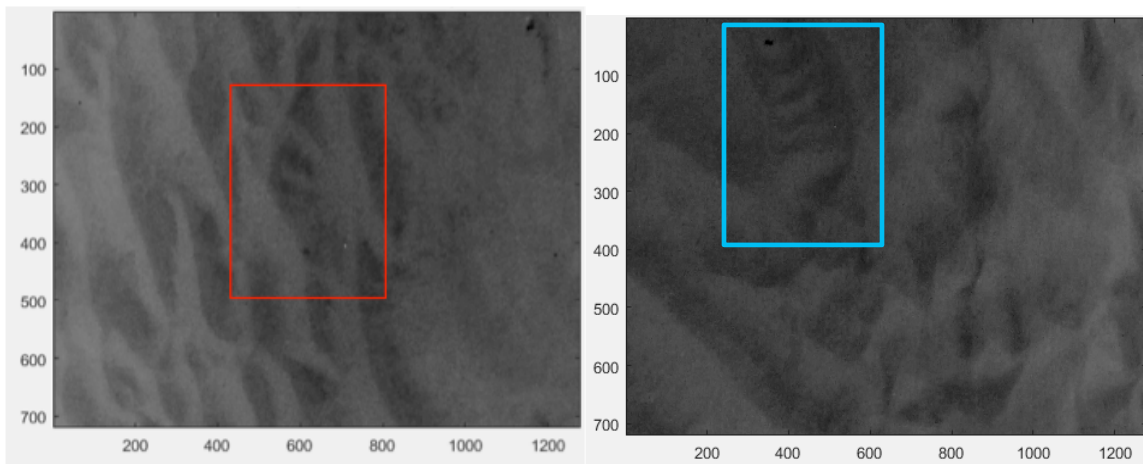


Figure 4.17 Photo from Nov. 15: 2m depth. (Left) Somewhat lunate, 3D ripples with flower-like structure indicated by red box. (Right) Isolated cross ripple forms indicated by blue box.

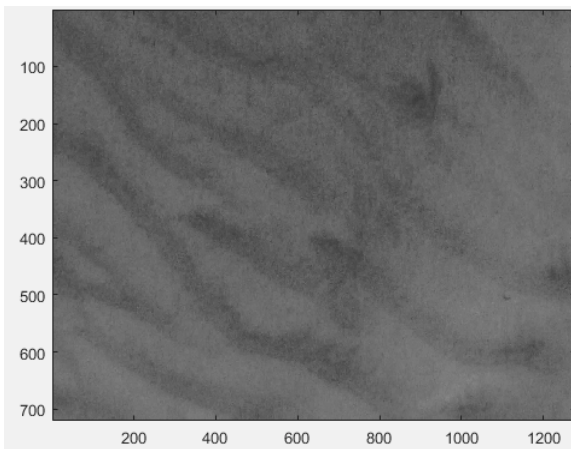


Figure 4.18 Photo from Nov. 15: 2.5 m depth. Ripples indicate a transition towards longer, more continuous bedforms.

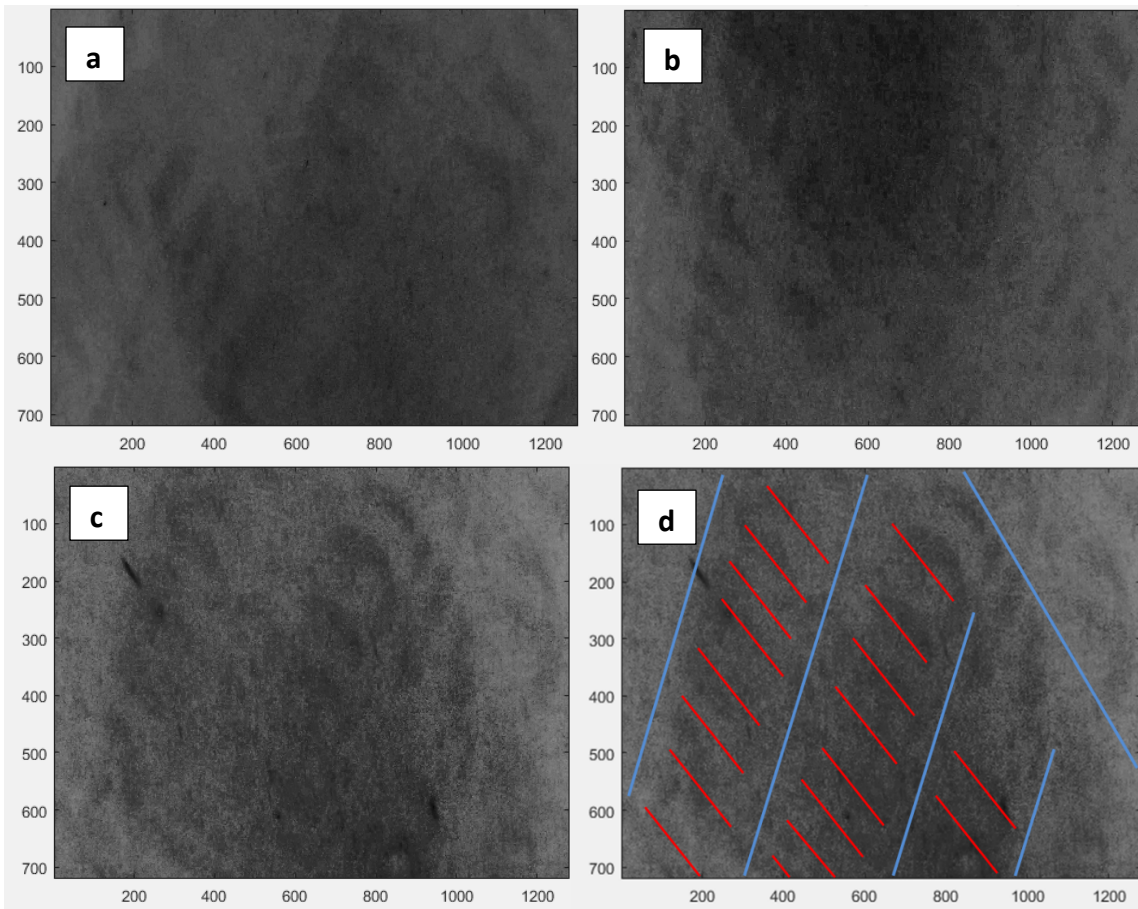


Figure 4.19 Photos from Nov. 17: 2m depth. Multiple examples of regular cross ripple structures crossing each other to form diamond shapes. Photo d is an enhanced repeat of photo c, showing long, straight, uninterrupted crests are outlined in blue, troughs of short wavelength, short-crested ripples outlined in red.

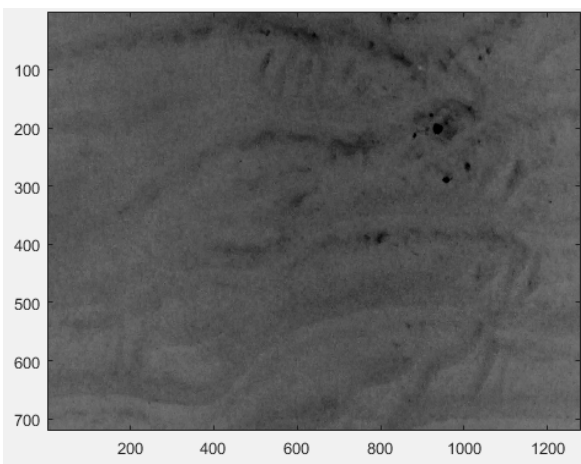


Figure 4.20 Photo from Nov. 26: 2m depth. Continuous, sinuous, long-crested ripples with some isolated sections of cross ripples.

Ripples preceding the storm event between 3–3.5m were long, relatively straight, well developed (larger wavelength), and continuous (Figure 4.21a). Ripples

branched off of each other irregularly, i.e. bifurcated, forming a zebra-stripe pattern. During the storm event, 3D cross ripples could be identified, but they were irregular, randomly oriented, and small compared to the cross ripples at 2–2.5m depth (Figure 4.21b). Wave motion was observed to affect the bed at 3m depths during the wave conditions of this storm event. During larger wave heights observed on November 22, the water column was overwhelmed by small bubbles, and showed large quantities of suspended sediment (Figure 4.22). After the storm, ripples were generally straight and continuous, but with sharper crests than ripples at this depth before the storm event. Ripple bifurcations were again present, forming a pattern resembling zebra stripes. There were isolated islands recurring somewhat regularly in the troughs of ripples at this depth (Figure 4.23).

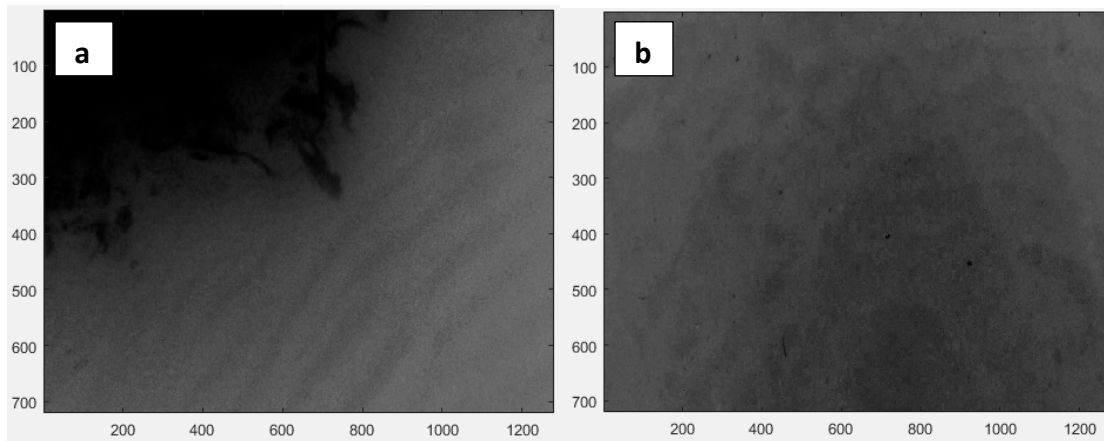


Figure 4.21 (a) Photo from Nov. 15: 3.5m depth. Long-crested, relatively straight ripples with bifurcations forming a zebra-stripe pattern. Dark, irregular shaped object in the top left corner of the photo is the edge of a cluster of growing seaweed. (b) Photo from Nov. 17: 3m depth. Cross ripple forms, less continuous and defined

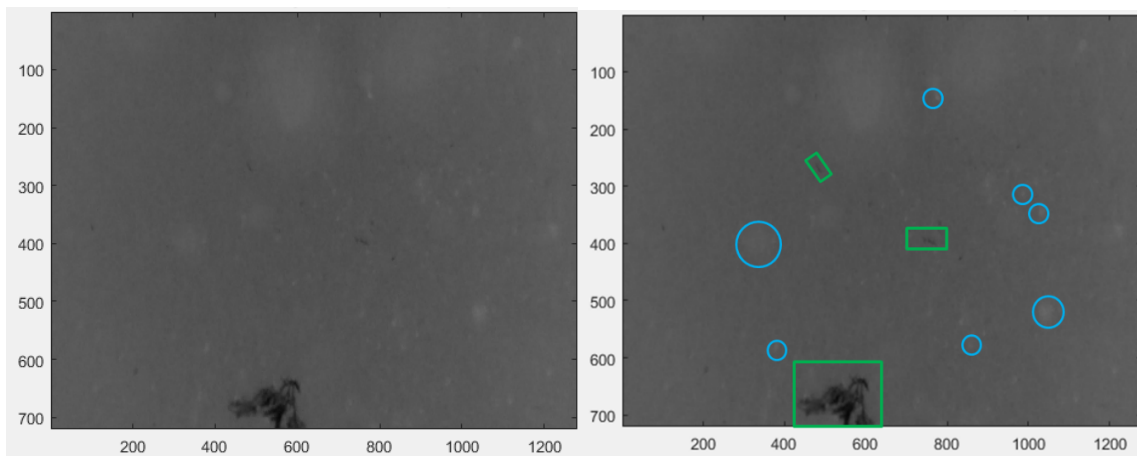


Figure 4.22 Photo from Nov. 22: 3m depth. Very turbid water column showing high quantities of bubbles (some examples indicated by blue circles), as well as suspended seaweed fragments (green rectangles).

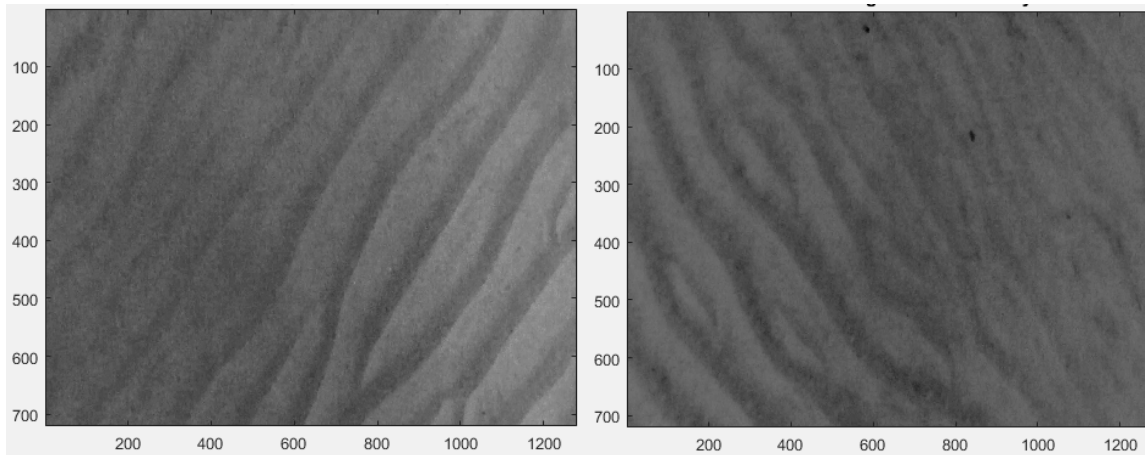


Figure 4.23 Photo from Nov. 26: 3m depth. (Left) Straight, continuous ripples with sharp crests and several clear bifurcations. (Right) Isolated short-crested ripples recurring somewhat regularly in the troughs of other ripples.

For colour images of ripples included in Section 4.4, see Appendix C.

Chapter 5: Discussion

5.1 Bedforms Observed and Interpretation

The repeated sequence of bed states reported by Clifton et al. (1971), Hay and Mudge (2005), Cheel (2007), and Cheel and Hay (2008), associated with growth and decay of storm conditions, was represented by the bedforms recorded in this study. An ‘outer planar facies’ similar to that of Clifton et al. (1971) was observed in the region of wave build up at depth of approximately 1m, just before waves broke onshore. This area displayed characteristics described by Clifton and co-workers, including gentle, irregular undulating ripples becoming planed off by wave action (illustrated by Figure 4.12), as well as long-crested very short wavelength linear transition ripples recorded in videos from November 17th. Farther seaward at 2m depths, there was a distinct occurrence of cross ripples during storm conditions recorded on November 17th. Pre- and post-storm bedforms in this area displayed irregular ripple forms with isolated cross ripples. The presence of similar features in pre-storm assessments may be attributed to the high-energy event on November 13th, where wave heights reached a maximum of 3.8m, and wind speeds peaked at 13.4 m/s (48.2 km/h). Lunate megaripples and cross ripples are

discussed in greater detail below. As predicted in models by Clifton (1976) and confirmed by Hay and Mudge (2005), seaward of the cross ripple zone at approximately 2.5m depth ripples in pre- and post-storm videos transition to irregular forms. Ripples observed in videos at 3m depths were characterized by a repeated 'zebra-pattern', paralleling descriptions by Clifton (1976) of long-crested ripple crests that sporadically bifurcate, or divide into branches.

There were no distinct lunate megaripples observed in the GoPro images. According to Hay and Mudge (2005), lunate megaripples, unlike other ripples, once formed persist through a variety of forcing conditions indicating a longer response time and evolution out of equilibrium with the forcing mechanisms. Clifton (1976) observed the formation of lunate megaripples in medium to coarse-grained sand under long period waves. He also inferred that lunate megaripples appeared to require a certain stability of currents to develop. Wind speed, wave heights, and resulting energies were variable throughout the duration of the storm event. In fact, there were almost two storm events recorded in this study: the first on November 17, with average wind speeds of 5.4 m/s (19.44 km/h) winds and peak wave heights of 2.2m; and a second on November 22, with average wind speeds of 10.24 m/s (36.86 km/h) winds and peak wave heights of 4.5m. In addition, the most abundant grain diameters of the sediment at Crystal Crescent Beach, measured during summer months, were 250–300 μ m. This diameter range classifies as fine to medium-grained sand under the Wentworth grain size classification scheme (Boggs 2012). Perhaps lunate megaripples were not formed during the storm event recorded in this study because sediment was too fine grained to support megaripple structures, and storm-forcing conditions were not consistent enough for the ripples to reach equilibrium and sustain their form.

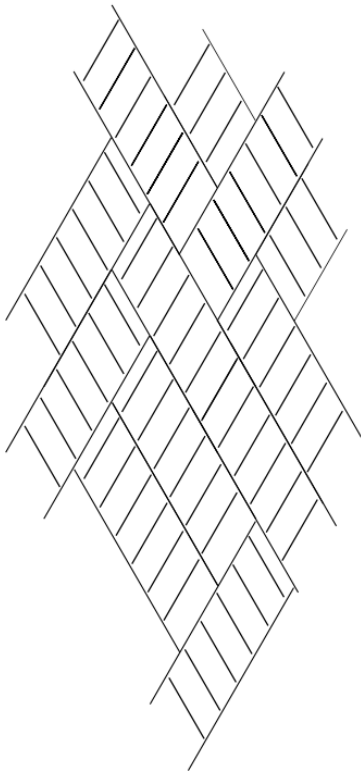


Figure 5.1 Representative sketch of cross-rippled bed with two long-crested components oriented at $\pm 30^\circ$, showing the incident wave direction (arrow) (Cheel & Hay).

Consistent with Cheel and Hay's (2008) study, cross ripples were observed create a diamond-shaped pattern, occurring at two dominant orientations that intersected at approximately 60° . The short crested ripples were also concordant with their observations, intersecting the long-crested component at 30° angles (Figure 5.1).

Sharper 'points' at the end of the diamond formed V's that converged around obstacles, such as vegetation embedded in the seafloor. Lab experiments conducted by Cheel (2007) displayed similar patterns. When a pipe was inserted into the ripple cart, cross ripples formed on either side of it. Cheel proposed that (1) localized obstacles in the

bed, which disturb the nearbed flow, may be responsible for the initiation of cross ripples and (2) the short-crested facet of these ripples might result

from flow parallel to long-crested aspect. This was considered in analysis of the GoPro videos, and projected in the schematic diagram below (Figure 5.2). Cross-ripples in the GoPro videos appeared to form around obstacles in the bed before propagating towards the beach. Shoreward migration of these ripples was also discerned by Clifton (1976).

The GoPro videos showed interesting relationships between waves, wave heights, and energy imparted to the seabed. In videos from November 15th, 17th and 22nd, more aggressive shoreward motion of sediment at the bed was observed compared to seaward motion. As water waves approach shore, the crest becomes sharper and narrower relative to the trough. Water beneath the crest moves more rapidly to maintain mass balance, producing stronger and more abrupt shoreward flow beneath the crest at the seafloor. This results in stronger shoreward transport of sediment under the crest compared to the seaward transport under the troughs as

observed in the GoPro videos. Clifton (1976) described a dependence of grain movement on velocity. Waves with larger heights and longer periods exert higher stresses on the seabed, and can affect the bed in deeper water. When wave heights averaged 1.1m on November 15th, videos indicated sediment mobilization at 2m depths, while the seafloor at 3m was unaffected by wave action. On November 17th, when larger wave heights averaged 1.8m, videos showed intensified motion of sediment at 2m, as well as mobilization and shoreward transport of sediment at a depth of 3m. Since sediment at depths of 2m and 3m are approximately the same in modal grain diameter, it is likely that the difference in wave influence was the primary factor causing the variability in sediment motion. Analyses of GoPro video from November 17th storm conditions also showed shoreward sediment motion at the bed lagging behind motion of suspended sediment and seaweed fragments occurring at the surface. This may be explained by descriptions of shoaling waves. As waves progress towards shallower water, the base of the wave comes in contact with the seafloor and slows due to friction (Marshak 2012). Thus, the part of the wave nearer to the sea surface would have passed beneath the GoPro lens prior to movement of sand grains at the seabed (Figure 5.3).

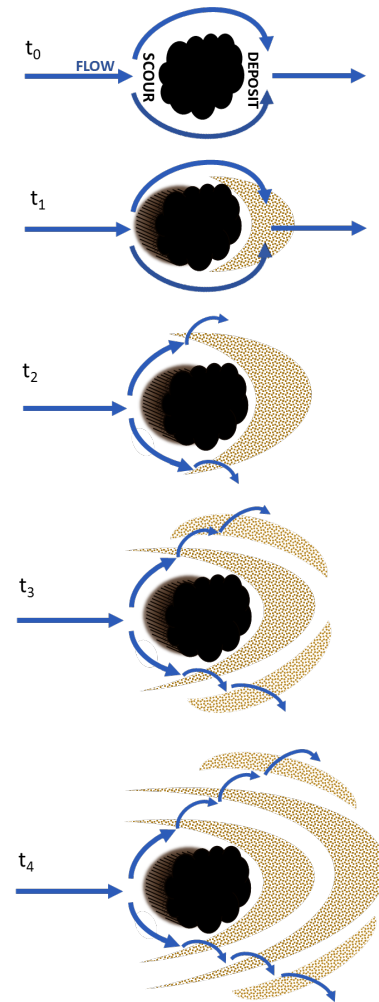


Figure 5.2 Original schematic diagram showing the potential correlation between obstacles at the seabed and cross ripple formation. Symbol t_0 indicates initial time or beginning of the process, while increasing values of 't' express passing time.

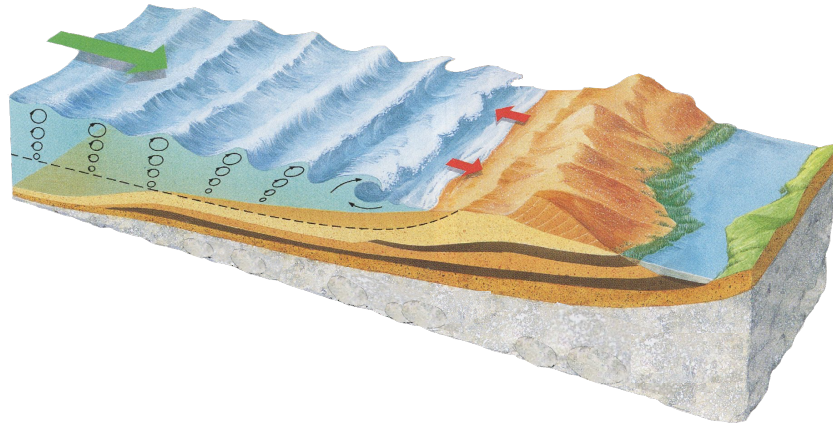


Figure 5.3 Schematic diagram of waves interacting with the seabed as they approach shore, showing how the base of the wave slows with respect to the portion of the wave at the surface. The green arrow indicate the propagation direction of incident waves, while red arrows show wave motion on the beach. Modified from (Marshak 2012).

5.2 Deeper Fishfinder 3.0 Sonar

The Deeper Fishfinder Sonar device did not provide any data from November 26th, when wave heights reached maximums of 4.9m. While in the field, the Deeper application on the cell phone projected depths between 4 and 8m – much greater than depth recorded in the previous two days. In GoPro videos on this day, no bedforms were identifiable, even when Saturation and Exposure settings were adjusted in Final Cut Pro. Instead, videos showed suspended sediment, vegetation fragments, and bubbles throughout the water column. Sonar operates by emitting low frequency sound waves that reflect off the seafloor and return to the sonar transducer. The time between emission and reception of the sound waves is measured with distance to a reflector determined from the speed of sound. Sound in water travels at 1400–1600 m/s, but sound in air moves much slower at 331.5 m/s (Burger et al 2006). The air bubbles observed in the water column slowed the speed of the sound waves emitted by the sonar device, resulting in a large, and erroneous depth measurement.

Several of the images created using data from the Deeper Fishfinder showed greater depth values than expected. These depths may be a result of the sonar's positioning. If the device was tipped on an angle relative to the seafloor, sound waves

would have a longer path to the sand than if the device was lying flat on the sea surface, which would result in a larger measurement for depth (Figure 5.4).

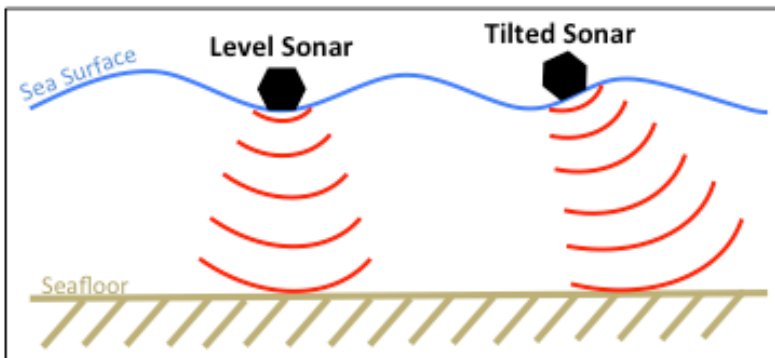


Figure 5.4 Original representative sketch showing positioning of Deeper Fishfinder sonar relative to the seafloor and effect on sound wave travel path. The level sonar shows sound waves' direct path to the sand, while the tilted sonar shows a lengthened path to the sand.

Figures 4.7 and 4.10(2) from November 17, 2017, when wave heights were larger than pre-and post-storm surveys, show a rapid depth increase after entering the water. Data points at 3.5–5m depths

irregularly overlap with data points from 1–2m depths. This is likely a result of rough wave conditions, causing the sonar device to be constantly tipping back and forth. The filled in “valley” features (blue to purple colour) extending to the shoreline in Figures 4.7 and 4.10(2) may be a result of the Matlab program interpolating to fill in spaces in the data.

5.3 Challenges

There were many challenges associated with fieldwork and the technologies used for this study. The android device, whether Samsung Tablet or cellphone, sometimes had difficulty maintaining Bluetooth connection with the Deeper 3.0, which was required for obtaining along-track GPS positions. This problem was a result of water resting on the android carrying case, which was at first a dry-bag. A Pelican case replaced the dry-bag, until water entered the case and damaged the Tablet. Following this event, the Tablet was unusable, and research was carried out using a Samsung Galaxy cell phone in a watertight case within the Pelican box.

When water was turbid, the Deeper 3.0 device showed uncharacteristic water depth measurements. Data showed a water depth much deeper than the apparent depth observed by the researcher at the surface. In addition, the device lagged when

sending measurements to the Samsung phone making it difficult to interpret the measured depth at which bedforms were observed.

Although the onset of autumn and winter months resulted in increased storm activity, which was useful for this investigation, the shorter days resulted in a narrow time window for obtaining useful video images of the seabed with the GoPro. When the sun was at a low angle relative to the horizon, the video images were more difficult to interpret, and bed features were not easily identified. Cloudy weather is also very common in Nova Scotia during this time of year, further hindering clarity of GoPro images. In addition, Crystal Crescent Beach Provincial Park closed in October making it more difficult to access the study site, and decreasing water temperatures made it difficult to obtain sand samples at depth.

Chapter 6: Summary and Conclusions

This study explored the potential for studying mobile bed adjustment in high-energy nearshore environments without disturbing the bed with an easily relocatable, mobile surface vehicle that could be operated in a range of wave conditions, while also functioning in shallow water. An old surfboard, used in the past for scientific research, was repurposed as a platform for mounting a GoPro Hero3 video camera, a Deeper Fishfinder Sonar, and an android cellphone or Tablet in waterproof casing. The video camera allowed for the pictorial recording of bedform geometries, while the sonar and android logged latitude, longitude, depth, and time data. Data was collected before a storm event, then twice during the storm under different wave conditions, and again after the event to observe the change in bedform geometries throughout growth and decay of storm wave conditions. Sand samples were collected from the beach at multiple depths for comparison grain size and mineralogical composition, while weather data was documented using NOAA buoy recordings.

Comparisons of hourly wind speed and wave height from before, during and after the storm showed that wave heights generally increased with wind speed. Analysis of depth data confirmed that the overall geometry of the seafloor was altered by the storm event, and the shape of the beach had varying highs and lows throughout the survey. Ripples were observed in 3 of the 4 GoPro videos. The pre-storm video showed a flat bed, planar facies at the shore, small somewhat lunate ripples with coarse sediment in the troughs as depth increased, then sections of isolated cross ripples, irregular ripples, and finally straight, continuous, elongated ripples that bifurcated. The first storm video (moving from the shoreline seaward) showed small wavelength, relatively straight ripples closest to the shore, then irregular cross ripples and obstacles in the bed, then very regular cross ripples producing diamond-like shapes, then less regular cross ripples at greater depths. In the second storm video, high quantities of bubbles, suspended sediment and pieces of seaweed prevented the recording of any ripple information. The post-storm video showed domes and depressions, like pockets, filled with coarse-grained sediment, then small scale lunate megaripples, then sigmoidal

ripples with isolated cross ripples, irregular ripples transitioning towards straight, long-crested, bifurcating ripples at depth. These results were consistent with previous bedform studies, as bed geometries showed a repeated shoreward progression and change corresponding to growth and decay of storm waves.

This study has demonstrated that it is possible to obtain observations of bedform patterns and water depth, allowing for identification of distinct ripple geometries and changes in overall bed state in a range of wave conditions, using a low-cost, easily relocatable, human-powered surface vehicle. The surface vehicle was operable in almost the full range of water depths encountered in nearshore environments i.e. from depths of several meters in the wave shoaling region offshore, as well as shoreward across the surf zone to less than 0.5m depths at the shore break and seaward edge of the swash. In future developments similar technologies could be made an integral part of the surfboard, in such a way that the structure of the board is maintained. Surfboard-surface-vehicles could then be implemented in surf-able sized waves and sent into the high-energy nearshore with a group of surfers to obtain simultaneous measurements over a wider area of the beach.

Referenced Literature

Boggs, S. 2012. Principles of sedimentology and stratigraphy fifth edition. Pearson Prentice Hall, Upper Saddle River, N.J.

Burger, H.R., Sheehan, A.F., Jones, C.H. 2006. Introduction to applied geophysics exploring the shallow subsurface. W.W. Norton & Company, Inc., New York, N.Y.

Cheel, R.A. 2007. Cross ripple occurrence in nearshore sands. M.Sc. thesis, Department of Oceanography, Dalhousie University, Halifax, N.S.

Cheel, R.A., Hay, A.E. 2008. Cross-ripple patterns and wave directional spectra. *Journal of Geophysical Research*, **113**.

Clifton, H.E. 1976. Wave-formed sedimentary structures – A conceptual model. *Beach and Nearshore Sedimentation*, **24**: 126–148.

Clifton, H.E., DIngler, J.R. 1984. Wave-formed structures and paleoenvironmental reconstruction.

Clifton, H.E., Hunter, R.E., Phillips, R.L. 1971. Depositional structures and processes in the non-barred high-energy nearshore. *Journal of Sedimentary Petrology*, **41**: 3, 651–670.

Hay, A.E., Mudge, T. 2005. Principal bed states during SandyDuck97: Occurrence, spectral anisotropy, and the bed state storm cycle, *Journal of Geophysical Research*. **110**.

Hutton, J., Craig C.Y. 1987. The 1785 abstract of James Hutton's theory of the earth. Scottish Academic Press. Edinburgh, Scotland.

Lackey, J.S., Erdman, S., Hark, J.S., Nowak, R.M., Murray, K.E., Clarke, D.B., Valley, J.W. 2011. Tracing garnet origins in granitoid rocks by oxygen isotope analysis: examples from the South Mountain Batholith, Nova Scotia. *The Canadian Mineralogist*, **49**: 417–439.

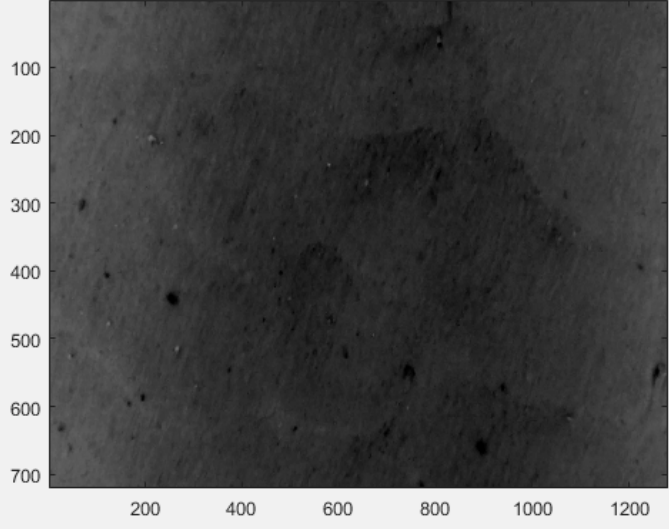
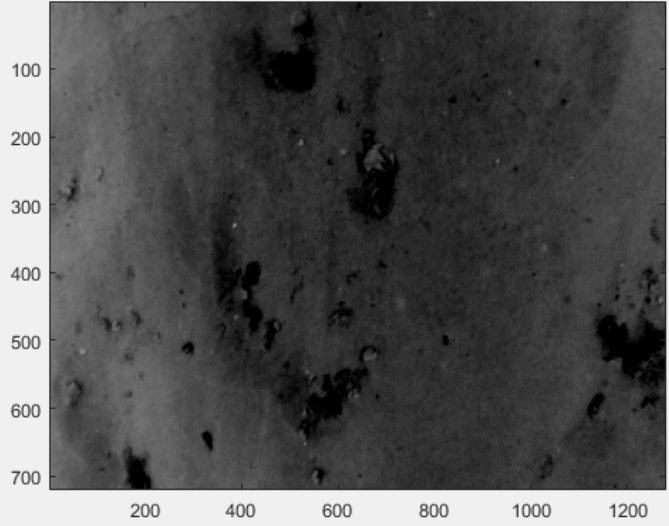
Marshak, S. 2012. Earth: Portrait of a planet 4th edition. W.W. Norton and Company, Inc., New York, N.Y.

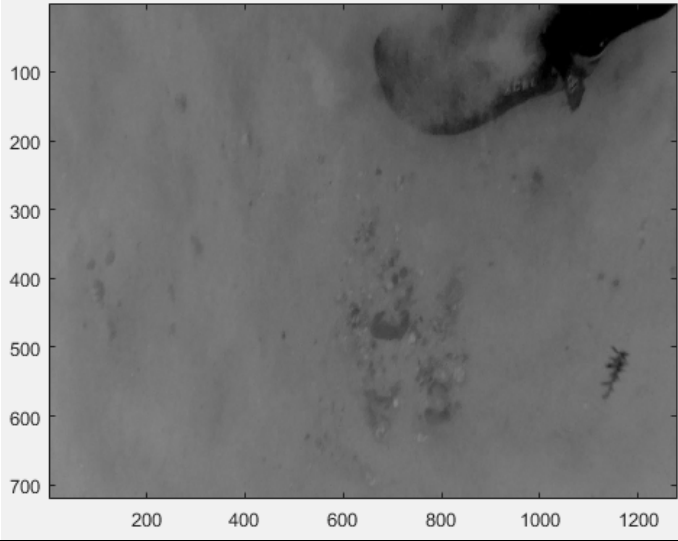
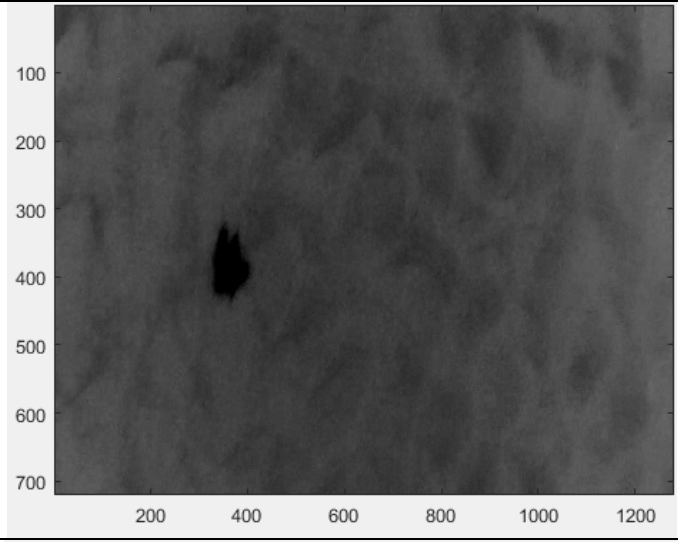
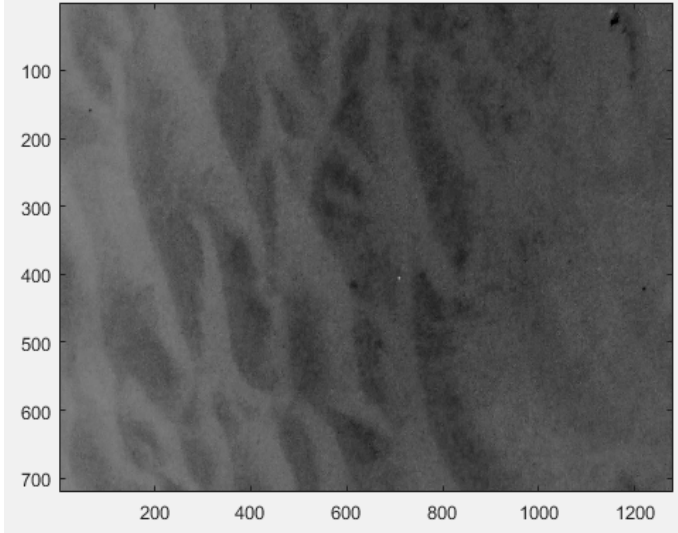
Reineck, H.-E., Singh, I.B. 1980. Depositional sedimentary environments with reference to terrigenous clastics. Springer-Verlag, Berlin, Heidelberg.

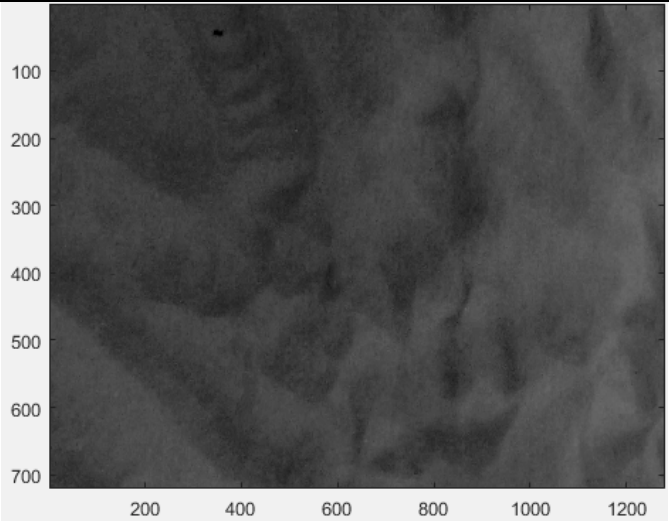
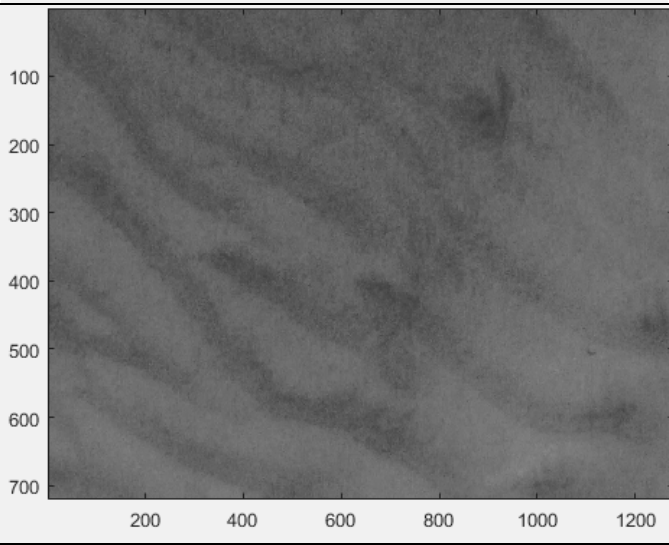
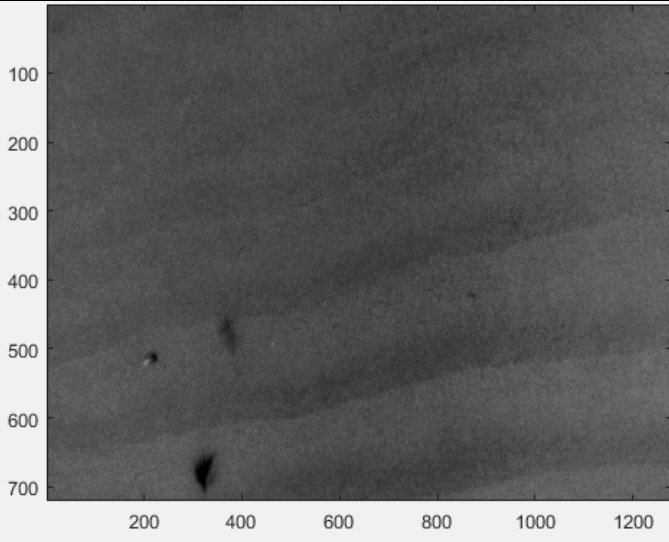
World Sea Temperature. 2017. Global sea temperature: Chester average August sea temperature [online]. Available from <https://www.seatemperature.org/north-america/canada/chester-august.htm> [cited 26 December 2016].

Appendix A. Photos of Bedforms from the GoPro

Scale: 200 pixels : 12.4cm

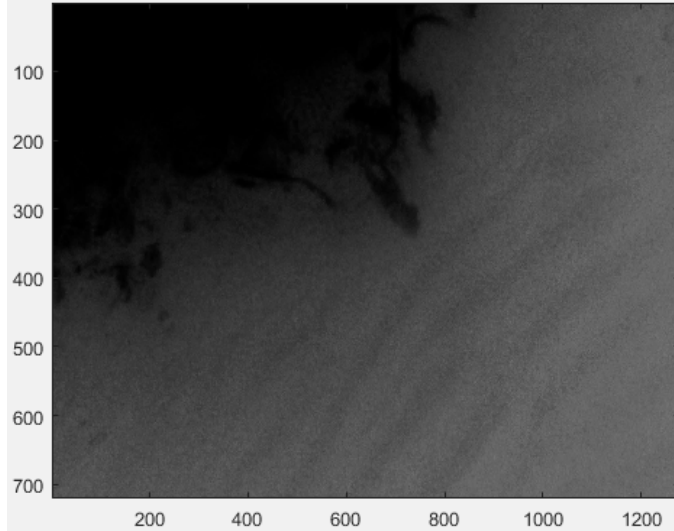
Fieldwork November 15, 2017	
<p>Nov. 15/16 1m depth</p> <p>Relatively low wavelength ripples crossed by thin linear structures oriented perpendicular to shore.</p>	
<p>Nov. 15/16 1m depth</p> <p>Somewhat lunate ripples with coarse grained (pebble sized) sediment in the troughs.</p>	

<p>Nov. 15/16 1m depth</p> <p>Image of foot/wetsuit boot ___m across, used for calculation of scale.</p>	
<p>Nov. 15/16 1.5m depth</p> <p>Black irregularly shaped object is a small plant in the sea bed.</p>	
<p>Nov. 15/16 2m depth</p> <p>Showing flower- like structures discussed in observations.</p>	

<p>Nov. 15/16 2m depth</p> <p>Isolated cross-ripple forms.</p>	
<p>Nov. 15/16 2.5m depth</p> <p>Transition towards longer, more continuous bedforms.</p>	
<p>Nov. 15/16 3m depth</p> <p>Long-crested, continuous ripples. Dark objects unknown.</p>	

Nov. 15/16
3.5m depth

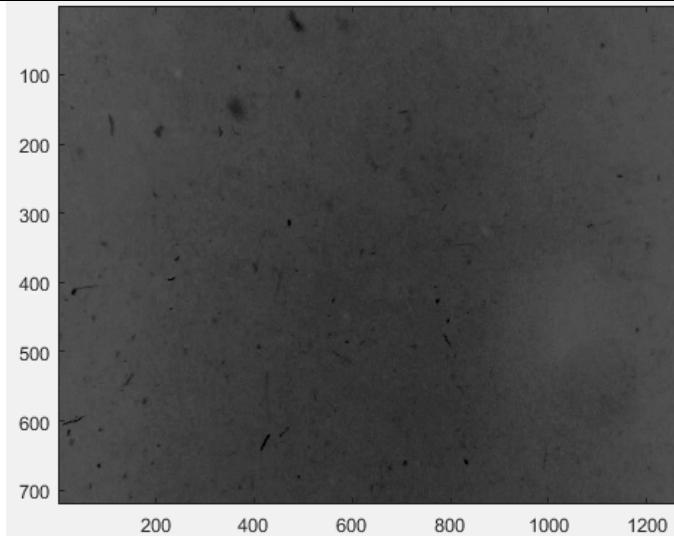
Dark, irregular shaped object I in the top left corner of the photo is the edge of some sort of reef or cluster of growing seaweed.



Fieldwork November 17, 2017

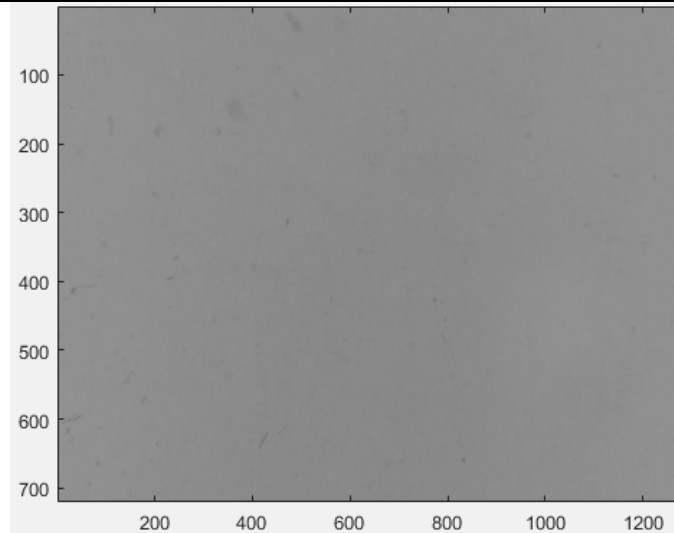
Nov. 17/16
1m depth

Photo showing highly turbid water near the swash zone.



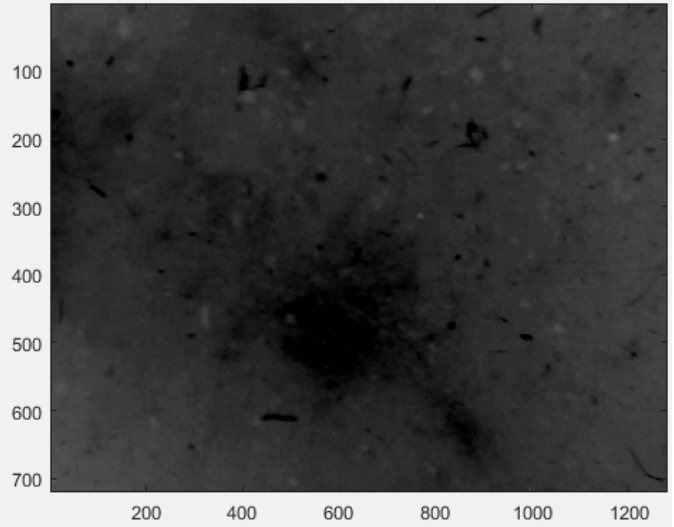
Nov. 17/16
1m depth

Repeated figure above. Shown without editing Exposure or Saturation in Final Cut Pro.



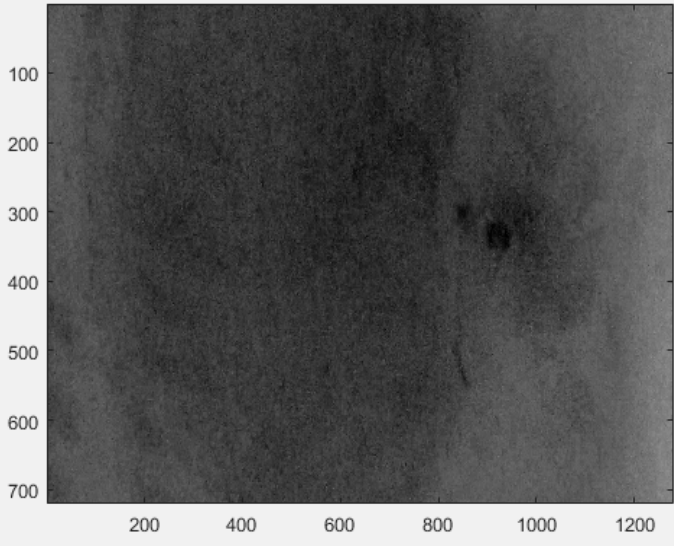
Nov. 17/16
1m depth

Photo showing highly turbid water near the swash zone.



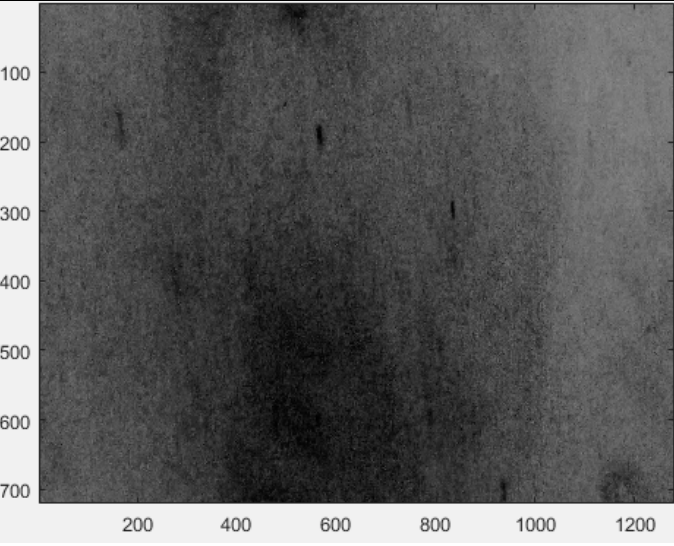
Nov. 17/16
1m depth

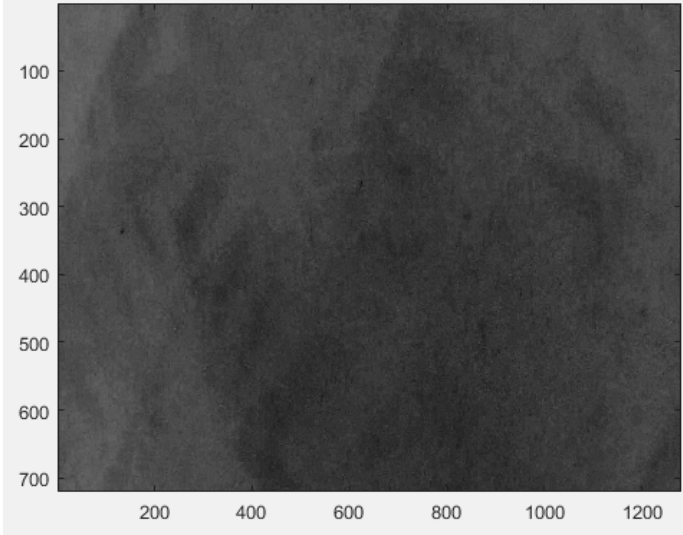
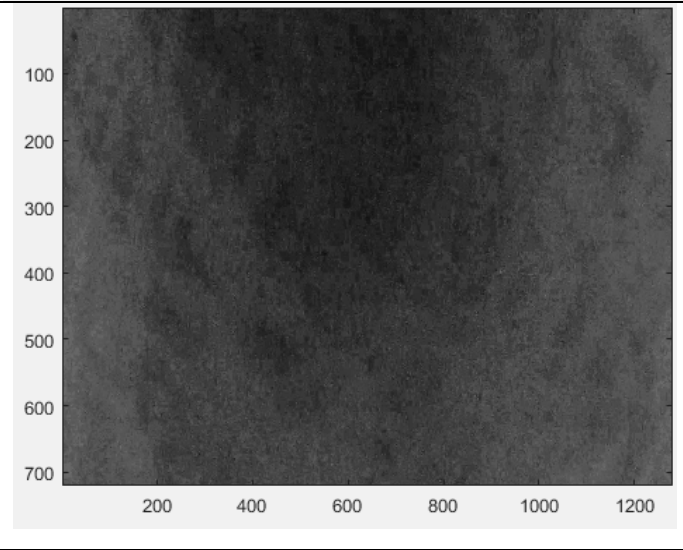
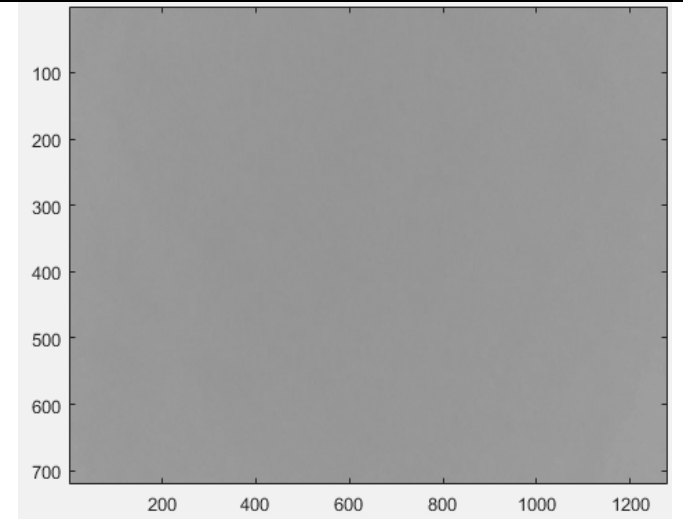
Two black circular features are small plants embedded in the seafloor surrounded by distinct cross ripples on the left side of the photo.

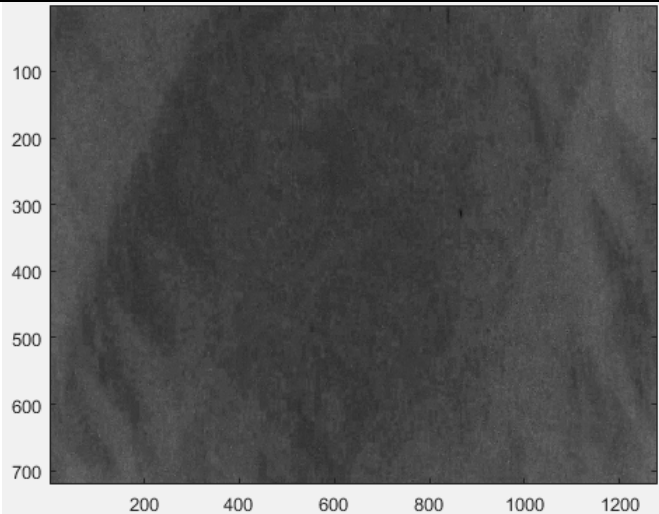


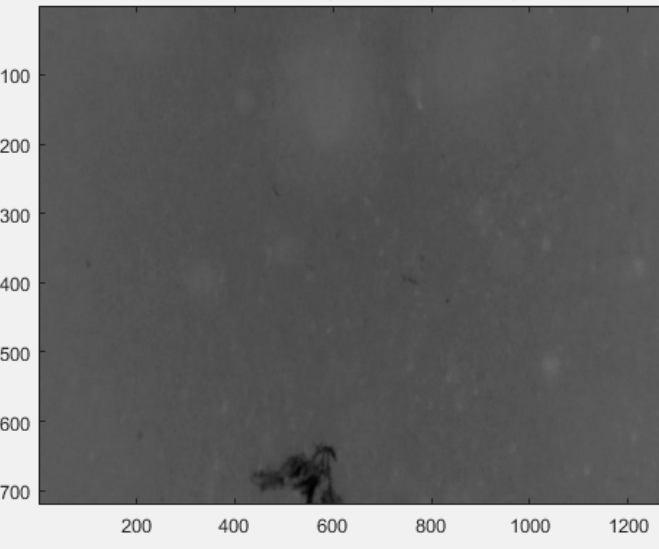
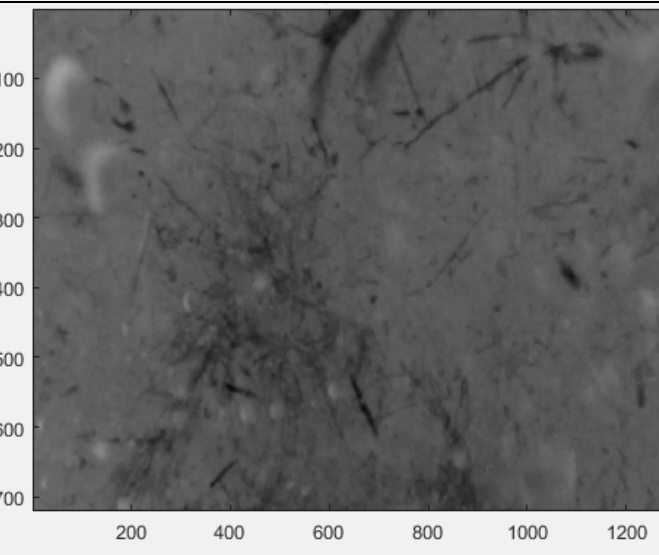
Nov. 17/16
1m depth

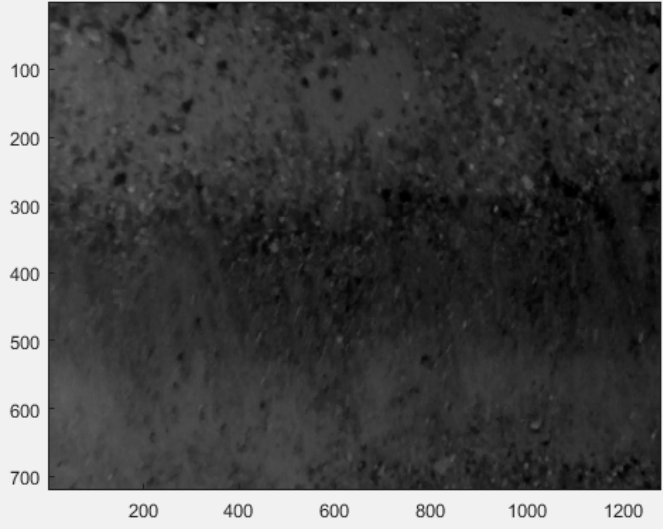
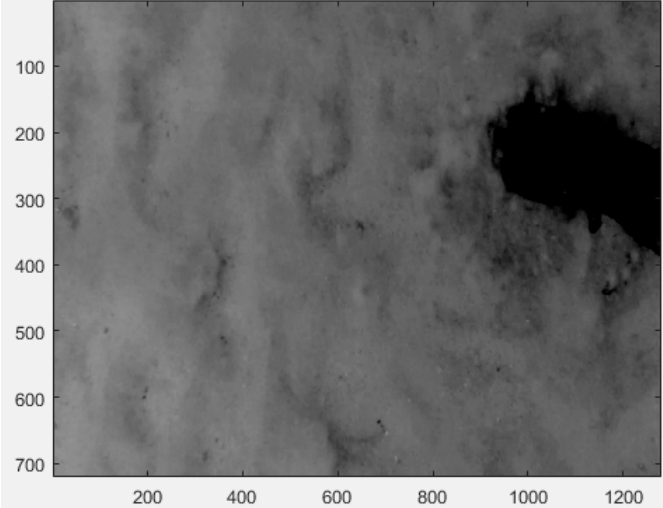
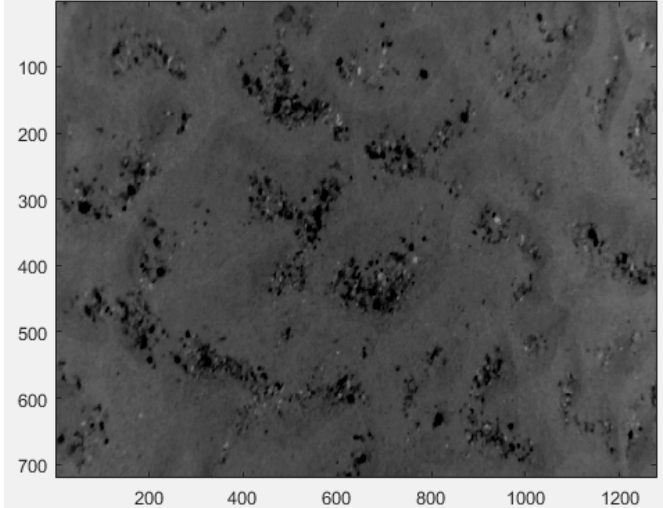
Multiple small plants in the sea bed (see Figure ___). Complex crossing of bedforms are observed to converge around this obstacles in the seabed.



<p>Nov. 17/16 2m depth</p> <p>Regular cross ripple sets intersecting each other to create large "V shapes".</p>	
<p>Nov. 17/16 2m depth</p> <p>Regular cross ripple bedforms with long-crested segments intersecting to create V shapes. Shadow at the top of the photo observed to result from the surfboard.</p>	
<p>Nov. 17/16 2m depth</p> <p>Repeated figure above. Shown without editing Exposure or Saturation in Final Cut Pro.</p>	

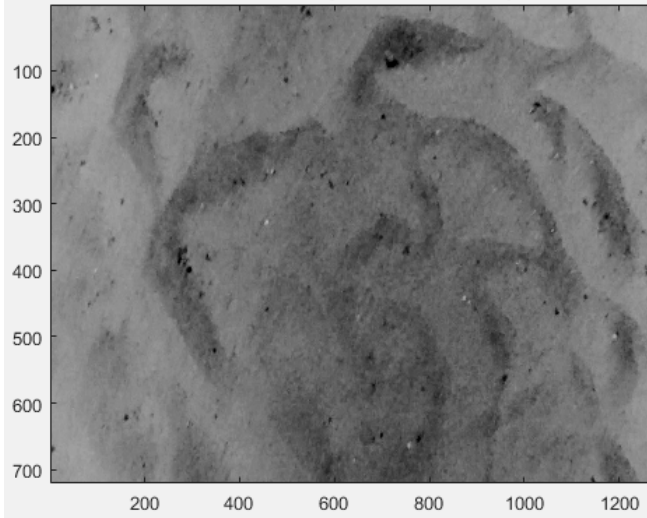
<p>Nov. 17/16 Approximately 2m depth</p> <p>Regular cross ripple bedforms</p>	
---	--

Fieldwork November 22, 2017	
<p>Nov. 22/16 3m depth</p> <p>Vey turbid water column showing high quantities of bubbles (white “blurs” in the photo), as well as suspended seaweed fragments.</p>	
<p>Nov. 22/16 Unknown depth</p> <p>Vey turbid water column showing high quantities of bubbles (white “blurs” in the photo), as well as suspended seaweed fragments.</p>	

Fieldwork November 26, 2017	
<p>Nov. 26/16 Swash Zone</p> <p>Coarse grained material collected at crests.</p>	
<p>Nov. 26/16 1m depth</p> <p>Image of foot/wetsuit boot ___m across, used for calculation of scale.</p>	
<p>Nov. 26/16 1.5m depth</p> <p>Three dimensional ripples with coarse grained (pebble sized) sediment in their troughs.</p>	

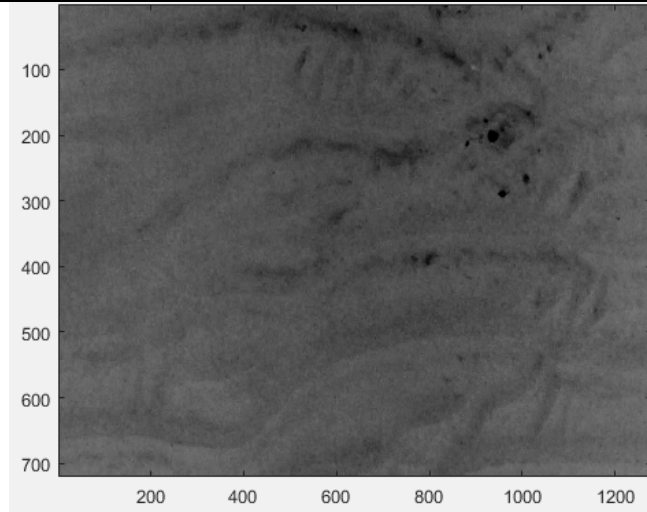
Nov. 26/16
1.5m depth

Small scale
lunate ripples.



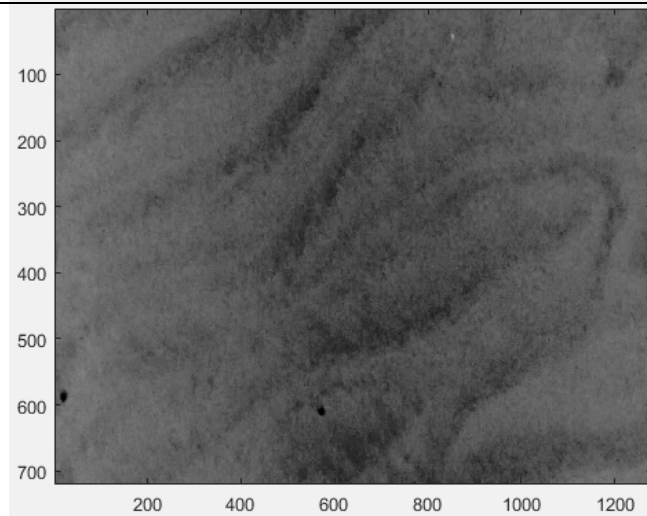
Nov. 26/16
2m depth

Continuous, long-
crested ripples
with some
isolated sections
of cross ripples.



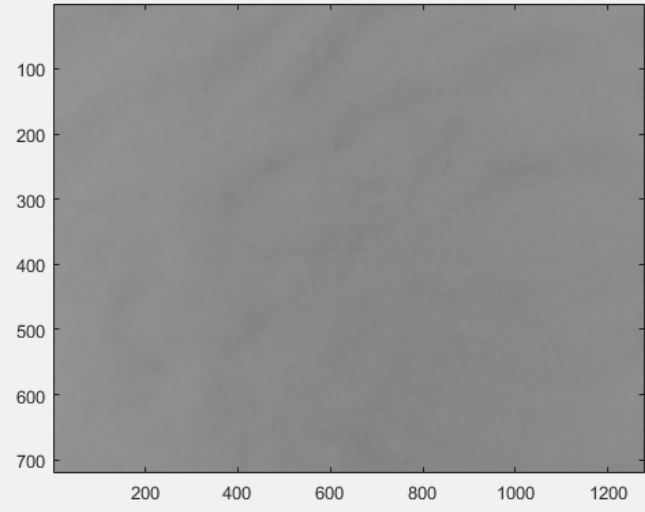
Nov. 26/16
2m depth

Complex ripple
shapes.



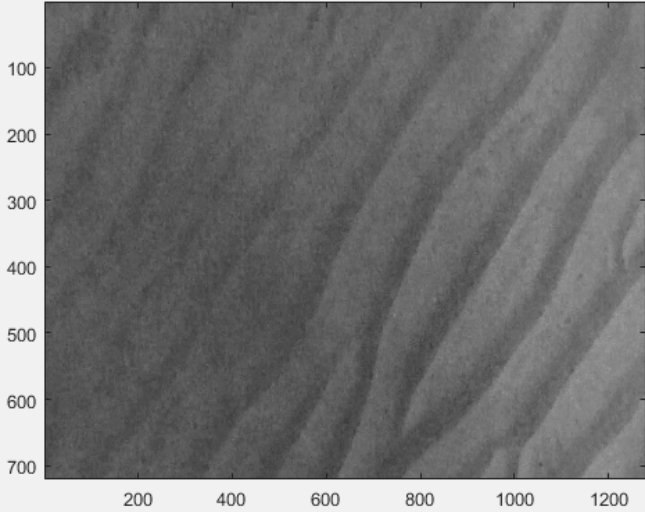
Nov. 26/16
2m depth

Repeated figure
above. Shown
without editing
Exposure or
Saturation in
Final Cut Pro.



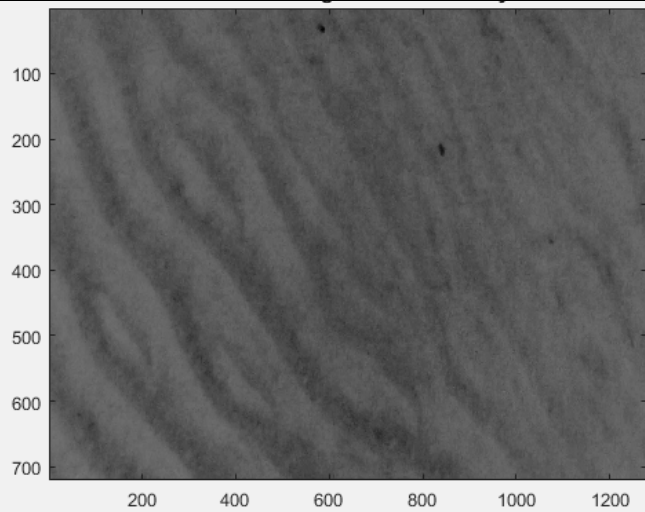
Nov. 26/16
3m depth

Long-crested,
continuous
ripples. Sharper
crests and
smaller
wavelengths than
ripples of at this
depth from
before the storm
event.



Nov. 26/16
3m depth

Sand "islands"
within other
ripple troughs.



Appendix B. Enhancements to Still Frames in Final Cut Pro

Field Work Nov. 15 (FWNOV15)

FWNOV15_1.5m_EDITED (and UNEDITED)

- Exposure → Increasing the shadows by moving the circle entitled “Shadows” down to -71%, then moving the “Midtones” circle up to 12%
- Saturation → Increasing the shadows by moving the circle entitled shadows down to -28%

FWNOV15_1.5m_2_EDITED (also UNEDITED)

- Saturation: Shadows -48%, Midtones 37%
- Exposure: Shadows -76%, Midtones 6%, Highlights 8%

FWNOV15_2m_EDITED (also UNEDITED)

- Saturation: Shadows -62%, Midtones 10%
- Exposure: -Shadows 58%, 12%

FWNOV15_between2and3m_EDITED

- Saturation: Shadows -93%, Midtones 65%, Highlights 49%
- Exposure: Shadows -82%, Midtones 25%

FWNOV15_3m_EDITED

- Saturation: Shadows -66%, Midtones 94%, Highlights 100%
- Exposure: Shadows -67%, Midtones 6%

FWNOV15_2m_2_EDITED

- Saturation: Shadows -73%, Midtones 12%
- Exposure: Shadows -49%, Midtones 63%, Highlights 25%

FWNOV15_3.5m_EDITED (also UNEDITED)

- Saturation: Shadows -65%,
- Exposure: Shadows -86%, Midtones 22%

FWNOV15_3.5m_2_EDITED

- Saturation: Shadows -61%, Midtones 20%
- Exposure: Shadows -60%, Midtones 3%

FWNOV15_1m_EDITED

- Saturation: Shadows -56%, Midtones 65%, Highlights 100%
- Exposure: Shadows -72%, Midtones 9%

FWNOV15_1m_2_EDITED

- Saturation: Shadows -56%, Midtones 65%, Highlights 100%
- Exposure: Shadows -72%, Midtones 9%

FWNOV15_1m_3_EDITED

- Saturation: Shadows -37%, Midtones 25%, Highlights 33%
- Exposure: Shadows -66%, Midtones 10%

FWNOV15_1m_foot_EDITED

- Saturation: Shadows -36%
- Exposure: Shadows -41%, Midtones 10%

FWNOV15_1m_footruler_EDITED

- Saturation: Shadows -36%
 - Exposure: Shadows -41%, Midtones 10%
- FWNOV15_between1and2m_EDITED
- Saturation: Shadows -41%
 - Exposure: Shadows -75%, Midtones 13%
- FWNOV15_3m_2_EDITED
- Saturation: Shadows -61%, Midtones 100%, Highlights 100%
 - Exposure: Shadows -74%, Midtones 12%
- FWNOV15_3m_2_EDITED
- Saturation: Shadows -89%, Midtones 100%, Highlights 100%
 - Exposure: Shadows -77%, Midtones 17%
- FWNOV15_1.5m_3_EDITED
- Saturation: Shadows -89%, Midtones 100%, Highlights 100%
 - Exposure: Shadows -77%, Midtones 17%
- FWNOV15_1.5m_4_EDITED
- Saturation: Shadows -89%, Midtones 100%, Highlights 100%
 - Exposure: Shadows -77%, Midtones 19%
- FWNOV15_2m_3_EDITED
- Saturation: Shadows -89%, Midtones 100%, Highlights 100%
 - Exposure: Shadows -79%, Midtones 19%
- FWNOV15_2m_4_EDITED
- Saturation: Shadows -83%, Midtones 100%, Highlights 100%
 - Exposure: Shadows -80%, Midtones 19%, Highlights 3%
- FWNOV15_2.5m_EDITED
- Saturation: Shadows -94%, Midtones 59%, Highlights 37%
 - Exposure: Shadows -86%, Midtones 22%, Highlights 6%

Field Work Nov. 17 (FWNOV17)

- FWNOV17_2m_EDITED (also UNEDITED)
- Saturation: Shadows -100%, Midtones 100%, Highlights 100%
 - Exposure: Shadows -79%, Midtones 13%, Highlights 1%
- FWNOV17_2m_interactionwithbottom_EDITED
- Saturation: Shadows -100%, Midtones 100%, Highlights 100%
 - Exposure: Shadows -76%, Midtones 13%, Highlights 6%
- FWNOV17_1m_highlyrubid_EDITED (also UNEDITED)
- Saturation: Shadows -100%, Midtones 100%, Highlights 100%
 - Exposure: Shadows -70%, Midtones 9%, Highlights 6%
- FWNOV17_1m_EDITED (also UNEDITED)
- Saturation: Shadows -100%, Midtones 100%, Highlights 100%
 - Exposure: Shadows -79%, Midtones 13%, Highlights 1%
- FWNOV17_approx2m_EDITED
- Saturation: Shadows -91%, Midtones 100%, Highlights 100%
 - Exposure: Shadows -83%, Midtones 22%, Highlights 3%

FWNOV17_approx2m_2_EDITED

- Saturation: Shadows -96%, Midtones 100%, Highlights 0%
- Exposure: Shadows -84%, Midtones 17%, Highlights 4%

FWNOV17_approx2m_2_EDITED

- Saturation: Shadows -96%, Midtones 100%, Highlights 70%
- Exposure: Shadows -84%, Midtones 28%, Highlights 6%

FWNOV17_3m_EDITED

- Saturation: Shadows -100%, Midtones 0%, Highlights 0%
- Exposure: Shadows -73%, Midtones 5%, Highlights 4%

FWNOV17_2m_2_EDITED

- Saturation: Shadows -100%, Midtones 0%, Highlights 0%
- Exposure: Shadows -86%, Midtones 13%, Highlights 5%

FWNOV17_1m_EDITED (??)

- Saturation: Shadows -100%, Midtones 0%, Highlights 0%
- Exposure: Shadows -74%, Midtones 9%, Highlights 5%

FWNOV17_1m_2_EDITED

- Saturation: Shadows -100%, Midtones 0%, Highlights 0%
- Exposure: Shadows -88%, Midtones 17%, Highlights 5%

FWNOV17_2m_3_EDITED

- Saturation: Shadows -58%, Midtones 0%, Highlights 28%
- Exposure: Shadows -86%, Midtones 31%, Highlights 3%

FWNOV17_2m_4_EDITED

- Saturation: Shadows -96%, Midtones 0%, Highlights 28%
- Exposure: Shadows -91%, Midtones 32%, Highlights 10%

FWNOV17_1m_obstacle_EDITED

- Saturation: Shadows -100%, Midtones 100%, Highlights 100%
- Exposure: Shadows -97%, Midtones 14%, Highlights 14%

FWNOV17_1m_obstacle2_EDITED

- Saturation: Shadows -100%, Midtones 100%, Highlights 100%
- Exposure: Shadows -97%, Midtones 13%, Highlights 14%

FWNOV17_2m_5_EDITED

- Saturation: Shadows -100%, Midtones 100%, Highlights 100%
- Exposure: Shadows -73%, Midtones 6%, Highlights 3%

FWNOV17_2.5m_EDITED

- Saturation: Shadows -100%, Midtones 100%, Highlights 100%
- Exposure: Shadows -80%, Midtones 14%, Highlights 3%

Field Work Nov. 22 (FWNOV22)

First few photos, no editing (no settings/colours changed)

FWNOV22_3m_EDITED

- Saturation: Shadows 0%, Midtones 0%, Highlights 0%
- Exposure: Shadows -34%, Midtones 0%, Highlights 0%

Field Work Nov. 26 (FWNOV26)

FWNOV26_2m_EDITED (also UNEDITED)

- Saturation: Shadows -81%, Midtones 50%, Highlights 100%
- Exposure: Shadows -57%, Midtones 2%, Highlights 2%

FWNOV26_2m_2_EDITED (also UNEDITED)

- Saturation: Shadows -81%, Midtones 47%, Highlights 54%
- Exposure: Shadows -59%, Midtones 3%, Highlights 2%

FWNOV26_2m_3_EDITED

- Saturation: Shadows -81%, Midtones 47%, Highlights 54%
- Exposure: Shadows -59%, Midtones 3%, Highlights 2%

FWNOV26_3m_EDITED

- Saturation: Shadows -100%, Midtones 52%, Highlights 54%
- Exposure: Shadows -58%, Midtones 14%, Highlights 6%

FWNOV26_1.5m_EDITED

- Saturation: Shadows -100%, Midtones 52%, Highlights 54%
- Exposure: Shadows -58%, Midtones 14%, Highlights 6%

FWNOV26_1m_foot_EDITED

- Saturation: Shadows -100%, Midtones 49%, Highlights 54%
- Exposure: Shadows -49%, Midtones 23%, Highlights 2%

FWNOV26_2m_4_EDITED

- Saturation: Shadows -100%, Midtones 49%, Highlights 54%
- Exposure: Shadows -65%, Midtones 23%, Highlights 2%

FWNOV26_4m_EDITED

- Saturation: Shadows -100%, Midtones 49%, Highlights 54%
- Exposure: Shadows -69%, Midtones 23%, Highlights 2%

FWNOV26_2m_5_EDITED

- Saturation: Shadows -100%, Midtones 49%, Highlights 54%
- Exposure: Shadows -67%, Midtones 23%, Highlights 2%

FWNOV26_3m_2_EDITED

- Saturation: Shadows -100%, Midtones 49%, Highlights 54%
- Exposure: Shadows -71%, Midtones 23%, Highlights 2%

FWNOV26_inat3m_EDITED

- Saturation: Shadows -100%, Midtones 49%, Highlights 54%
- Exposure: Shadows -66%, Midtones 23%, Highlights 2%

FWNOV26_2m_6_EDITED

- Saturation: Shadows -100%, Midtones 49%, Highlights 54%
- Exposure: Shadows -65%, Midtones 23%, Highlights 2%

FWNOV26_snakehead3m_EDITED

- Saturation: Shadows -100%, Midtones 49%, Highlights 54%
- Exposure: Shadows -60%, Midtones 23%, Highlights 2%

FWNOV26_snakehead3m_2_EDITED

- Saturation: Shadows -100%, Midtones 100%, Highlights 100%

- Exposure: Shadows -53%, Midtones 23%, Highlights 2%

FWNOV26_1.5m_2_EDITED

- Saturation: Shadows -100%, Midtones 100%, Highlights 100%
- Exposure: Shadows -55%, Midtones 9%, Highlights 1%

FWNOV26_swash_EDITED

- Saturation: Shadows -100%, Midtones 100%, Highlights 100%
- Exposure: Shadows -55%, Midtones 9%, Highlights 1%

FWNOV26_swash2_EDITED

- Saturation: Shadows 0%, Midtones 0%, Highlights 0%
- Exposure: Shadows -14%, Midtones 0%, Highlights 0%

Appendix C. Colour Versions of Photos in section 4.4

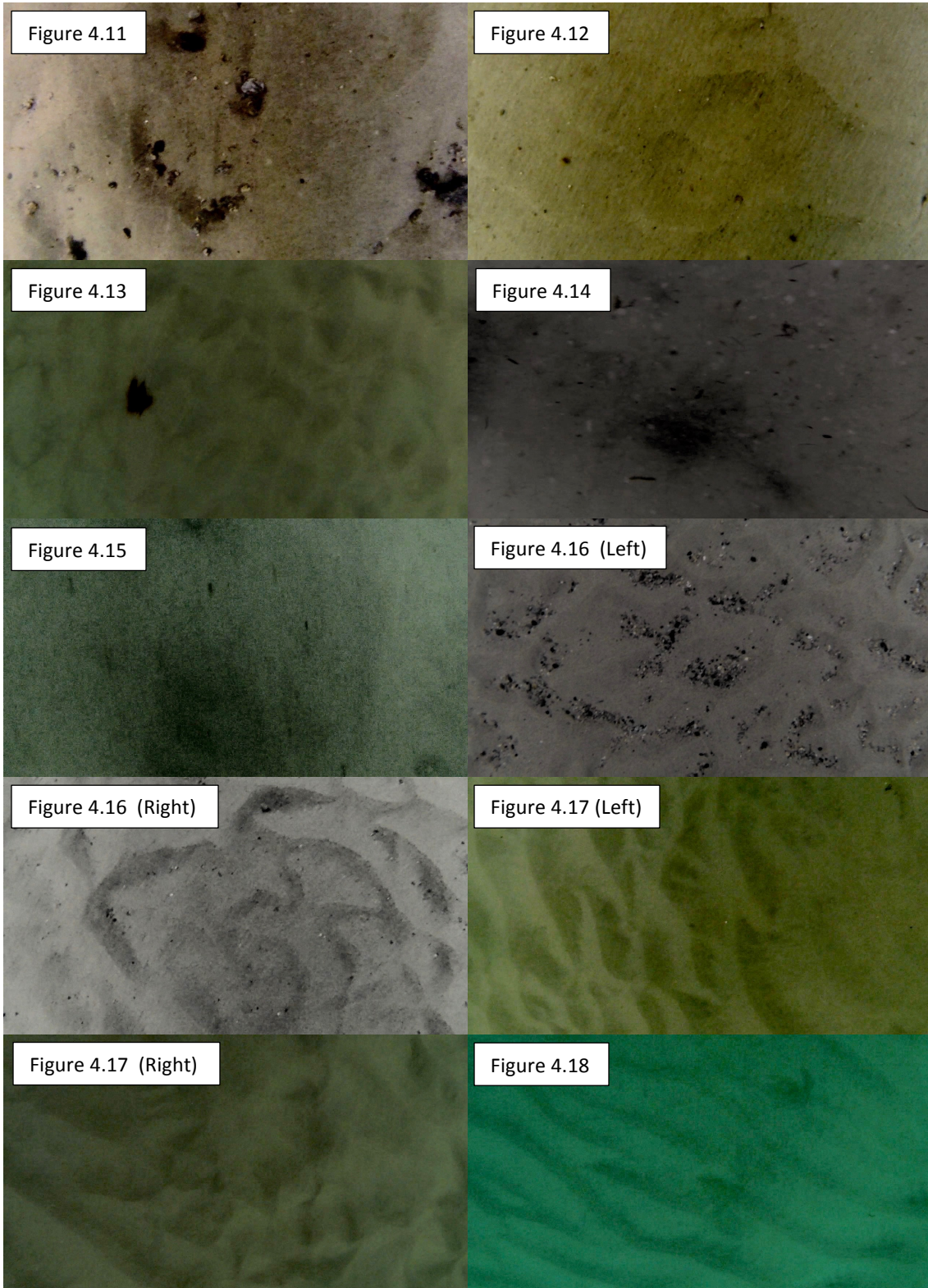




Figure 4.19a)



Figure 4.19b)



Figure 4.19c)

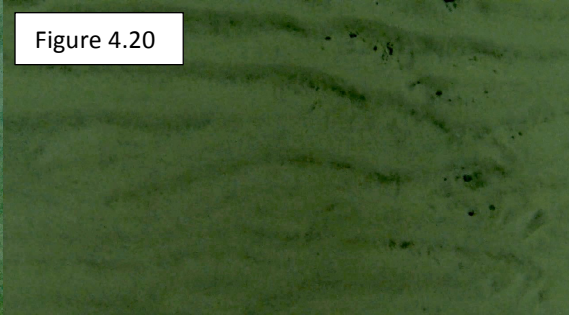


Figure 4.20)

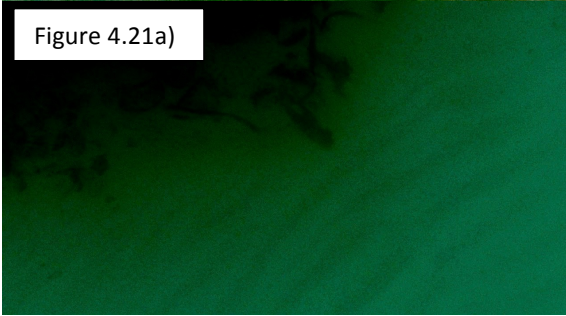


Figure 4.21a)

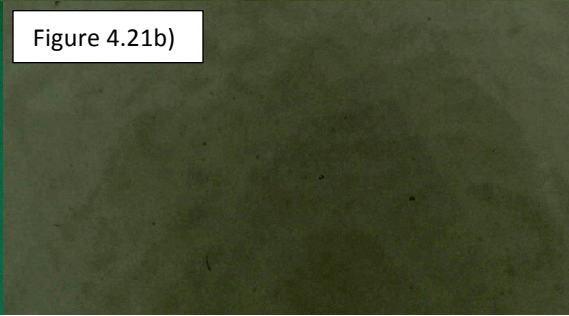


Figure 4.21b)



Figure 4.22)

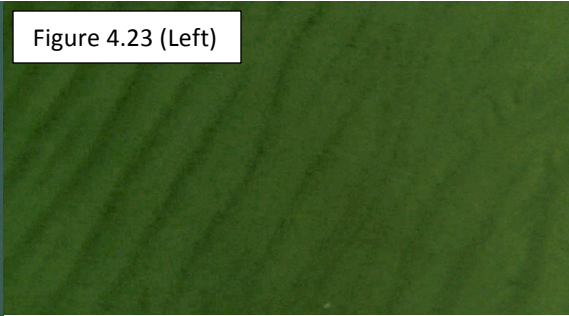


Figure 4.23 (Left)

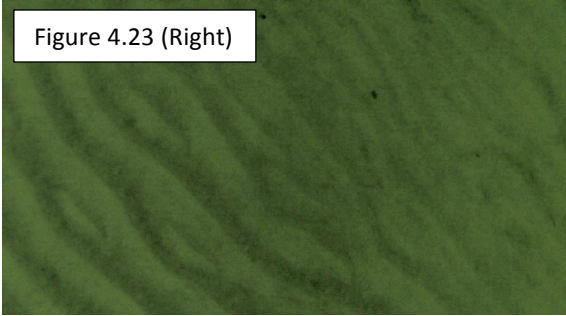


Figure 4.23 (Right)